*J. Fluid Mech.* (1994), *vol.* 271, *pp.* 17–53



# Self-excited oscillations in the wake of two-dimensional bluff bodies and their control

By MICHAEL SCHUMM[1], EBERHARD BERGER[1] AND PETER A. MONKEWITZ[2]

[1] Hermann Foettinger Institut for Fluid- and Thermodynamics, Technical University Berlin, D-10623 Berlin, Germany

[2] Department of Mechanical Engineering, Swiss Federal Institute of Technology, CH-1005 Lausanne, Switzerland

(Received 21 December 1992 and in revised form 7 January 1994)

The onset of Kármán-vortex shedding is studied experimentally in the wake of different two-dimensional bluff bodies, namely an oblong cylinder, circular cylinders and plates of rectangular cross-section. Different control measures, such as wake heating, transverse body oscillations and base bleed are investigated. As the steady-periodic Kármán shedding has previously been identified as a limit-cycle, i.e. as self-excited oscillations, the experiments are interpreted in the framework of the Stuart–Landau model. The coefficients of the Stuart–Landau equation for the characteristic vortex shedding amplitude, i.e. the linear temporal growth rate, linear frequency and the Landau constant, are fully determined for the two cylinders and in part for the plate. For this purpose transients are generated by suddenly switching transverse body oscillations or base bleed on or off. The analysis of these transients by a refined method based on complex demodulation provides reliable estimates of the model coefficients and yields an experimental validation of the concept that a global instability mode grows or decays as a whole. Also, it is demonstrated that the coefficients of the Stuart–Landau equation are independent of the experimental technique used to produce the transients.

## 1. Introduction

Over the last decade, the research on vortex shedding from bluff bodies has received new impulses from the theory of hydrodynamic instability. The concept of local absolute and convective instability in particular, pioneered by Briggs (1964) in the context of plasma instabilities, has proved useful in shear flows. The initial ideas about the possible connection between local absolute instability (Pierrehumbert 1984; Koch 1985; Huerre & Monkewitz 1985) and self-excited or time-amplified global oscillations of the entire near wake have been refined in a series of papers (Triantafyllou, Triantafyllou & Chryssostomidis 1986; Monkewitz & Nguyen 1987; Chomaz, Huerre & Redekopp 1988; Monkewitz 1988; Karniadakis & Triantafyllou 1989; Ohle & Eckelmann 1992; Noack 1992; Noack & Eckelmann 1994). To put the connection between local and global behaviour on a firm mathematical basis Huerre & Monkewitz (1990), Chomaz, Huerre & Redekopp (1991), Hunt & Crighton (1991), Soward (1992), Monkewitz, Huerre & Chomaz (1993) and Le Dizès *et al.* (1993, 1994) have used asymptotic methods based on the assumption that the streamwise evolution of the base flow is slow on the scale of a typical instability wavelength.

This development of asymptotic theories, however, would have remained rather

academic without the experimental discovery of Mathis, Provansal & Boyer (1984) and Provansal *et al.* (1987) that Kármán-vortex shedding is indeed a limit-cycle oscillation of the near wake, resulting from a time-amplified global instability. They showed that the wake dynamics could be described by a single Stuart–Landau (SL) equation (Stuart 1971; see also §2) by measuring all coefficients of the SL-equation for a range of Reynolds numbers near the onset of Kármán shedding. Guided by the SL-model, Mathis *et al.* designed for this purpose the first successful transient experiments, which consisted of measuring the response of the wake to an impulsive change of the free-stream velocity. Since then, experiments of this type have been repeated and refined by Sreenivasan, Strykowski & Olinger (1986), Strykowski & Sreenivasan (1990) and Schumm (1991) for the wake and by Raghu & Monkewitz (1991) for a heated jet.

The present paper is based on Schumm's thesis (1991) and gives extensive and more complete results, including SL-coefficients, for three different two-dimensional bluff bodies: an oblong cylinder, a circular cylinder and a blunt-based plate. To obtain the coefficients of the SL-equation by transient experiments, some means of control is required. In the following, we present results associated with control by variation of Reynolds number, wake heating, base bleed or suction and forced transverse cylinder oscillations. However, only the last two methods are used to produce transients by suddenly switching the control on or off. Other control measures not considered here include suppression of vortex shedding by splitter plates (Roshko 1954*a*, *b*), forcing by pulsating jets near the separation lines (Williams, Mansy & Amato 1992) and by rotational oscillations of the cylinder (Tokumaru & Dimotakis 1991). All the above control measures fall into the categories of 'steady modifications of boundary conditions' or 'open-loop forcing'. The effectiveness of the former measures has been firmly linked to changes in the degree of absolute instability in the near wake, with a sufficient reduction thereof leading to the suppression of vortex shedding (Monkewitz & Nguyen 1987; Huerre & Monkewitz 1990; Yu & Monkewitz 1990; Monkewitz 1993). The mechanism of vortex-shedding control by open-loop forcing, on the other hand, has so far eluded a general explanation. A third type of control, 'feedback or closed-loop control', is beyond the scope of this paper. In the wake, it has been explored experimentally by Berger (1964, 1967), Ffowcs Williams & Zhao (1989), Monkewitz, Berger & Schumm (1991), Roussopoulos (1993*a*, *b*) and has been modelled theoretically by Monkewitz (1989).

In §2, we briefly summarize the concept of local absolute instability, linear global modes and the SL-equation. In addition, a refined data reduction technique is described which yields improved estimates of the SL-coefficients. In §3 the different control measures are related to the stability-theoretical ideas of §2 and in §§4–6 we discuss the results pertaining to the oblong piezoceramic cylinder, the circular cylinder and the blunt-based plate, respectively. In the conclusions, the relation of the present measurements of SL-coefficients to analytical work is assessed.

## 2. Theoretical models for the evolution of Kármán vortex shedding

### 2.1. *Global instability and the Stuart–Landau model*

When considering the stability properties of a two-dimensional streamwise evolving flow, the so-called locally parallel approach is commonly used. For this, one takes the local mean velocity profile at a fixed streamwise location and considers the stability of a hypothetical parallel flow of infinite streamwise extent with a velocity profile equal to the selected local profile of the non-parallel flow. Obviously the selection of streamwise location for the locally parallel analysis is arbitrary and hence the

connection between the local analyses and the 'true' instability of the non-parallel flow remains unclear. In the context of linear stability this true instability is referred to as 'global mode'. It is simply a generalized time-harmonic solution (allowing for temporal growth or decay) of the governing equations, linearized around a non-parallel basic flow, say, $\bar{U}(x, y)$ in two dimensions. That is

$$U(x, y, t) = \bar{U}(x, y) + \hat{\boldsymbol{u}}(x, y) \exp(-\mathrm{i}\omega_G t) + O(|\hat{\boldsymbol{u}}|^2), \tag{1}$$

where $\omega_G$ is the complex global frequency. Depending on the sign of the imaginary part of $\omega_G$, the global mode is stable [$\mathrm{Im}(\omega_G) < 0$] or unstable [$\mathrm{Im}(\omega_G) > 0$]. Under the assumption that a typical instability wavelength $\lambda$ is much shorter than the distance $\mathscr{L}$ over which the basic flow changes significantly, i.e. that $\lambda/\mathscr{L} \equiv \epsilon \ll 1$, and that there is no long-range pressure feedback such as in edge-tone phenomena, Huerre & Monkewitz (1990), Chomaz *et al.* (1991), Soward (1992), Monkewitz *et al.* (1993) and Le Dizès *et al.* (1993, 1994) have shown that local absolute instability over some streamwise interval of the non-parallel flow is necessary for global instability. These analyses also imply that a disturbance, generated by a localized initial impulse, takes of the order of $\epsilon^{-1}$ times the period $2\pi/Re(\omega_G)$ of the instability wave to evolve into the mode shape $\hat{\boldsymbol{u}}(x, y)$ of the most unstable linear global mode. This latter evolution is of course only relevant if it takes place before nonlinear effects become important.

When considering nonlinear effects we can restrict ourselves, as shown by Mathis *et al.* (1984) and Provansal *et al.* (1987), to the case of a supercritical Hopf bifurcation (Stuart 1971), i.e. to the case when a linearly unstable global mode evolves continuously into limit-cycle oscillations. In this situation it is always possible to slow down the saturation process by positioning oneself sufficiently close to the linear global stability boundary. Near this boundary it is therefore meaningful to consider the evolution of an initial impulse in a non-parallel flow as a 'two-step' process: the first step consists of the impulse evolving into the most unstable linear global mode by the process of selective amplification, assuming that the 'critical' mode grows much faster than all the 'higher' global modes. The second step involves a period during which the linear global mode as a whole grows exponentially at the rate $\mathrm{Im}(\omega_G)$, followed by nonlinear saturation (see the recent analysis by LeDizès *et al.* 1993). For this scenario it is clear that, as soon as the linear global mode is established, the dynamics can be described by a single characteristic amplitude $A(t)$, associated with the fundamental frequency component, which satisfies an SL-equation near the onset of Kármán-vortex shedding,

$$\frac{\mathrm{d}A}{\mathrm{d}t} = [\sigma_r + \mathrm{i}\sigma_i](P)\, A - [l_r + \mathrm{i}l_i]\, |A|^2 A + O(|A|^5). \tag{2a}$$

In this equation, $P$ represents a bifurcation parameter such as the Reynolds number $Re$. The above concepts are broadly supported by the fully non-parallel stability analysis of the wake by Noack (1992), Ohle & Eckelmann (1992) and Noack & Eckelmann (1994) who developed a low-dimensional Galerkin model for the wake dynamics.

As discussed by Stuart (1971), the balance of terms in (2*a*) requires that the linear growth rate $\sigma_r$ be small of order $O(|A|^2)$ for a supercritical bifurcation, i.e. for $l_r > 0$. Hence the 'distance from criticality' $[P - P_{cr}]$ has to be of order $O(|A|^2)$, where $P_{cr}$ is defined by $\sigma_r(P_{cr}) = 0$, and it is consistent to approximate the coefficients in (2*a*) by

$$\left.\begin{aligned} \sigma_r &= [P - P_{cr}][\mathrm{d}\sigma_r/\mathrm{d}P](P_{cr}) + O(|P - P_{cr}|^2), \\ \sigma_i &= \sigma_i(P_{cr}) + [P - P_{cr}][\mathrm{d}\sigma_i/\mathrm{d}P](P_{cr}) + O(|P - P_{cr}|^2), \\ [l_r + \mathrm{i}l_i] &= [l_r + \mathrm{i}l_i](P_{cr}) + O(|P - P_{cr}|). \end{aligned}\right\} \tag{2b}$$

The coefficient $(\sigma_r + i\sigma_i)$ is thereby independent of location and $l$ is the first Landau 'constant'. From (2$a$) the saturation or limit-cycle amplitude for $P > P_{cr}$ is immediately obtained as

$$|A|_{sat} = [\sigma_r/l_r]^{\frac{1}{2}} = \{[\mathrm{d}\sigma_r/\mathrm{d}P](P_{cr})/l_r\}^{\frac{1}{2}}[P-P_{cr}]^{\frac{1}{2}}. \tag{3}$$

Introducing the modulus and phase of $A$ into (2$a$) finally leads to

$$\frac{1}{|A|}\frac{\mathrm{d}|A|}{\mathrm{d}t} = \sigma_r - l_r|A|^2 = \sigma_r(1-|A|^2/|A|^2_{sat}), \tag{4a}$$

$$\frac{\mathrm{d}\alpha}{\mathrm{d}t} = \sigma_i - l_i|A|^2 = \sigma_i - (\sigma_r l_i/l_r)|A|^2/|A|^2_{sat}; \quad A = |A|\exp[i\alpha]. \tag{4b}$$

The introduction of $|A|_{sat}$ in the above expressions pertains to the case $P > P_{cr}$ and serves to show that only the ratio $l_i/l_r$ is a true constant, independent of the location where $A$ is measured, since it is related to the nonlinear frequency shift. $l_r$ itself does depend on spatial location and corresponds to the saturated global mode shape $\hat{\boldsymbol{u}}(x, y)$ via equation (3).

The relations (4$a$) and (4$b$) show that the instantaneous growth rate $|A|^{-1}\mathrm{d}|A|/\mathrm{d}t$ and the instantaneous frequency $\mathrm{d}\alpha/\mathrm{d}t$ are linear functions of the square of the instantaneous amplitude $|A|^2(t)$. This allows a good error estimate of previous growth rate measurements typically obtained at amplitudes as large as half the saturation amplitude. Beyond this, the relations (4) can be used, as described below, to obtain improved values for the coefficients $\sigma$ and $l$ and, as a consequence, a more precise identification of the stability boundary $P_{cr}$.

So far no mention has been made of three-dimensional effects that have been the subject of much recent research by, among others, Gerich & Eckelmann (1982), Ramberg (1983), Williamson (1989, 1994), Eisenlohr & Eckelmann (1989), Hammache & Gharib (1991) and Albarède & Monkewitz (1992). The main point is that, given enough time, the end conditions have an influence over the entire span even of very long bluff bodies. In particular they determine the shedding angle and the long-time limit of the saturation frequency for Reynolds numbers below the transition to 'turbulence' (around 200 for the circular cylinder). For our purposes, the key word is 'given enough time'. As shown by the experiments of Williamson (1989) and the model of Albarède & Monkewitz (1992) the vortex shedding during a start-up is always two dimensional. It takes a finite time, which is proportional to the length of the cylinder, until the initial two-dimensional state at, say, the centre of the span 'feels' the end conditions. Hence, for the transient experiments in particular we do not have to concern ourselves with these three-dimensional effects. This claim is supported by flow visualization in §6.

### 2.2. *The processing of transient data*

For the present and most previous experiments the output of a single hot wire measuring the streamwise disturbance velocity has been chosen to characterize the global mode dynamics. The only practical requirement for the sensor is that it be placed in a region where the signal amplitude is not too small compared to the maximum amplitude and where probe interference is not a problem. For the wake this means that the probe must be placed sufficiently far downstream of the region of absolute instability, i.e. certainly downstream of the recirculating region. In some cases, however, a probe location in the unsteady potential flow, well to the side of the near wake, may also be appropriate.

Since the equations (4) pertain only to the fundamental frequency component, a raw

transient representing the growth and saturation of a global mode must first be band-pass filtered. For all the present results the transients $A_{raw}(t)$ were recorded on an HP 3562 Dynamic Signal Analyzer in time-capture mode. The signal was then filtered in the spectral domain. For this, the pass-band of the window $\mathrm{BP}(f)$ was in all cases centred on the Kármán-shedding frequency $f_K$ with a width of $\Delta f \approx f_K$ and a cosine taper over $0.15\Delta f$ on each side. The FFT of the real filtered signal was hence obtained as $\tilde{A}_r = \mathrm{BP}(f) \times \mathrm{FFT}(A_{raw})$.

Next, the problem of experimentally obtaining instantaneous growth rates and frequencies in a reliable fashion was approached by building the 'complex' amplitude $(A_r + \mathrm{i}A_i)(t)$ from the measured real signal $A_{raw}(t)$. The real part is thereby simply the band-pass filtered signal $A_r = \mathrm{FFT}^{-1}(\tilde{A}_r)$, while the imaginary part $A_i$ of the signal can be identified in the standard fashion with the Hilbert transform of $A_r$ which, in the spectral domain, amounts to multiplying each FFT component by $(-\mathrm{i})$. Hence we have

$$A_i = \mathrm{FFT}^{-1}(-\mathrm{i}\tilde{A}_r), \tag{5}$$

and the time derivatives of $|A| = [A_r^2 + A_i^2]^{\frac{1}{2}}$ and $\alpha = \tan^{-1}(A_i/A_r)$ in $(4a)$ and $(4b)$ can be evaluated by finite differences. In practice, the raw transients $A_{raw}$ are contaminated by noise and it is clear that the instantaneous experimental growth rates $|A|^{-1}\,\mathrm{d}|A|/\mathrm{d}t$ and frequencies $\mathrm{d}\alpha/\mathrm{d}t$ determined in this fashion are only reliable where the signal-to-noise ratio is significantly above unity, i.e. at finite amplitudes. However, the growth rates and frequencies can easily be extrapolated to their values $\sigma_r$ and $\sigma_i$ at infinitesimal amplitudes by fitting equations $(4a)$ and $(4b)$ to the data. The normalized Landau constant $(l_i/l_r)$, on the other hand, is obtained from the difference between the extrapolated linear frequency $\sigma_i$ and the frequency of the saturated limit cycle. As will be demonstrated in §4, this procedure leads to significant improvements of the SL-coefficients near the onset of Kármán vortex shedding. Further away from critical conditions it is the only promising method to analyse short transients which saturate in a few periods (see also Raghu & Monkewitz 1991). The more reliable coefficients are then used to test the 'two-step' scenario proposed above by comparing the dynamics at different spatial locations.

## 3. Methods for controlling Kármán vortex shedding in the near wake

With steady-periodic data only the relation (3) for the saturation amplitude can be verified. Hence one has to carry out transient experiments to fit the SL-model (2) to experimental data. This requires a control mechanism by which vortex shedding can be significantly reduced or suppressed in a stable manner under supercritical conditions $P > P_{cr}$ or can be stimulated when $P < P_{cr}$, i.e. when the natural wake is stable. Turning off the controller then allows the natural shedding to grow and saturate or the stimulated shedding to decay. In practice, a control mechanism, besides being reasonably simple to implement, has to satisfy several criteria in order to yield meaningful transients:

(i) For the instability to evolve on the 'proper' basic flow, the controller should not induce significant changes of the mean flow.

(ii) The 'switch-off time' of the controller has to be small compared to the e-fold growth- or decay-time of the transient. At the same time, switching the actuator on or off should not cause significant disturbances.

(iii) For $P < P_{cr}$ the controller has to induce vortex shedding with a frequency corresponding to the subcritical conditions.

In the following we discuss the control mechanisms which are used in the present experiments relative to the above requirements and highlight the connection with local stability properties.

### 3.1. *Change of Reynolds number*

The control method of choice in the past (Mathis *et al.* 1984; Sreenivasan *et al.* 1986; Provansal *et al.* 1987) has been the modification of the Reynolds number, i.e. impulsive changes of the free-stream velocity. The connection with the theoretical model of §2 has been established in detail by Monkewitz (1988), who showed how an increase in Reynolds number correlates with an increase in both the size of the region of local absolute instability in the near wake and in the magnitude of the maximum absolute growth rate. This method of producing wake transients satisfies the requirements (i) and (ii) reasonably well, although there appear to be problems with (ii) when reducing the Reynolds number from a supercritical to a subcritical value $Re < Re_{cr}$ (see Sreenivasan *et al.* 1986). When producing decaying transients, the method is also problematic because the frequency corresponding to the initial supercritical Reynolds number is arbitrarily imposed on the final subcritical state, thus violating (iii).

### 3.2. *Control wire*

The technique, proposed by Strykowski & Sreenivasan (1990), consists of introducing a thin control cylinder with a diameter of typically $\frac{1}{8}$ to $\frac{1}{20}$ of the primary cylinder and parallel to it into the wake. The most effective location for suppression of vortex shedding is generally in the shear layers bordering the mean recirculation region. Strykowski & Sreenivasan (1990) have shown numerically that experimentally observed suppression of vortex shedding corresponds to a globally damped wake. The effect of the control cylinder on local stability properties, however, can only be speculated upon. It is likely that it is primarily the breaking of the mean flow symmetry which is responsible for the reduction of absolute instability. This control technique is not suited to produce transients, as none of the criteria (i)–(iii) can be satisfied. We mention it here because it has a bearing on the placement of the heating wire in the recirculation region (see §§3.3 and 5).

### 3.3. *Wake heating*

It has been noted in the past (Noto, Ishida & Matsumoto 1985; Mori, Hijikata & Nobuhara 1986) that Kármán vortex shedding can be suppressed by heat addition to the near wake. The connection of this effect to local stability properties was investigated by Yu & Monkewitz (1990) who argued that the primary effect of heating was to reduce the density of the near wake, which in turn decreased local absolute growth rates. The issue is not entirely settled, though, as Lecordier, Hamma & Paranthoen (1991) suggest that the modification of Reynolds number by the heating is at least equally important in gaseous media. In §5 we report a few results pertaining to the saturation amplitude as a function of heat input, but again, the technique is unsuitable for the generation of transients because of thermal inertia.

### 3.4. *Base bleed*

Another well-known method for the suppression of vortex shedding from bluff bodies consists in bleeding fluid from the blunt base (Wood 1964, 1967; Bearman 1967). Again, the connection between suppression and local stability properties is given by the fact that absolute instability in the near wake is reduced very effectively by reducing or eliminating reverse flow (Monkewitz & Nguyen 1987; Monkewitz 1988). Base bleed control to produce experimental transients has been implemented for the first time by

Hannemann, Lynn & Strykowski (1986). The idea is to suppress vortex shedding completely at some supercritical Reynolds number by base bleed, which is then shut off impulsively by a solenoid valve. This technique has been further developed by Schumm (1991) and has been supplemented by 'base suction' which is ideally suited to induce global instability at normally subcritical Reynolds numbers, as shown in §6 for rectangular plates. Within limits, all the criteria (i)–(iii) can therefore be satisfied easily.

### 3.5. *Forced cylinder vibrations*

The use of forced cylinder oscillations for the reduction or suppression of Kármán-vortex shedding was first proposed by Berger (1964, 1967) and Wehrmann (1965) and has been perfected by Schumm (1991). The method uses small-amplitude transverse cylinder osillations, with displacements of a few percent of the cylinder diameter. The most effective suppression of vortex shedding was found for a harmonic forcing frequency of around 1.8 times the natural shedding frequency. As opposed to all the previous control measures which represented steady modifications of the boundary conditions, the control is achieved by open-loop forcing. The effect can therefore no longer be explained in terms of local stability properties that change in response to a modified basic flow, but is most probably the result of nonlinear interactions between the natural global instability and the forcing input. However, we know of no analysis to support this hypothesis.

The technique has proved particularly successful with an oblong piezoceramic cylinder for which all the requirements (i)–(iii) can be ideally satisfied, as demonstrated in the next section.

## 4. The wake of an oblong piezoceramic cylinder: control by forced transverse oscillations

### 4.1. *Experimental set-up*

For the following experiments the original oblong cylinder of Berger (1964, 1967), with a thickness $D = 0.69$ mm, a chord of 1.68 mm and a length $L = 70$ mm has been used. As shown in figure 1, it was mounted across the nozzle (diameter 100 mm) of a small open-return wind tunnel with a measured turbulence level of 0.2% in the free stream. The cylinder was made of piezoceramic material (used for gramophone styli) strung onto three very thin piano wires, which provided high torsional stiffness, and allowed us to tune its mechanical natural frequency. The two sides of the cylinder parallel to the free stream were coated with electrodes connected to binding posts via the 'V-struts' visible on figure 1 (*b*). By applying a sinusoidal voltage across the electrodes, the fundamental transverse bending mode of the cylinder could be excited. The fact that the resulting displacement was not constant along the span did not seem to have a discernible influence on the experiments (owing to the mounting on longer wires, any twisting of the cylinder was prevented and the amplitude at the ends was still about half the amplitude at the centre). This piezoceramic cylinder, which has also been called 'bimorph transducer', has turned out to be ideally suited for transients as it is highly damped after the excitation is turned off. This is demonstrated in figure 2 which shows the hot-wire signal at $(x/D, y/D) = (10, 1)$ for a supercritical Reynolds number of 83 ($Re_{cr} = 79.2$) together with the voltage across the cylinder electrodes. As long as the forcing signal at 560 Hz is applied, the vortex shedding with a saturated frequency of 313 Hz is completely suppressed, as evidenced by the corresponding power spectrum. When the excitation is turned off, the cylinder acts as a transducer and the trace of

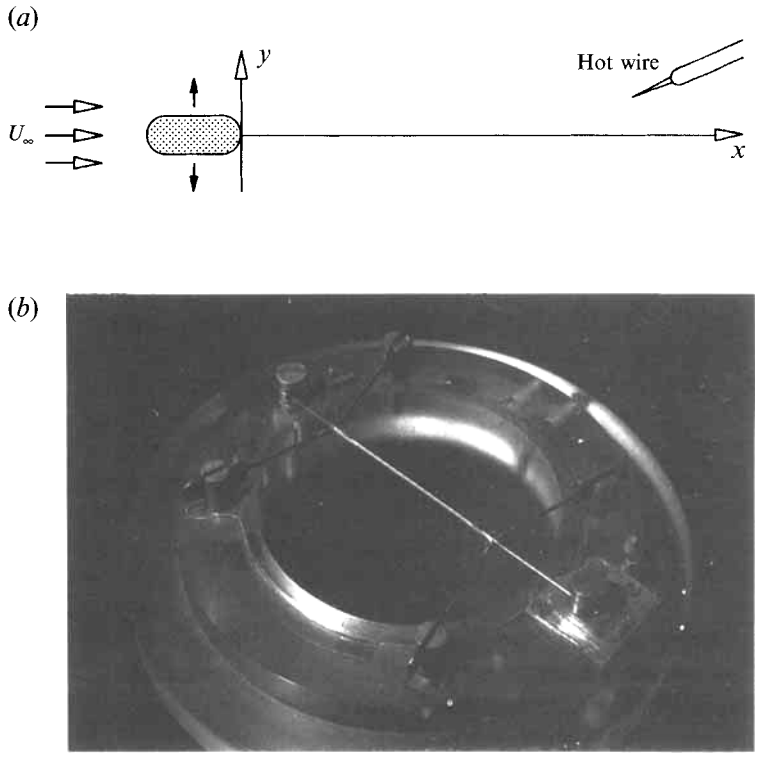


FIGURE 1. (*a*) Schematic of the oblong piezoceramic cylinder. (*b*) Photograph of its mounting across the nozzle of the wind tunnel.

figure 2(*b*) provides an estimate of about 20 ms for the time constant of the structural damping. At the same time the Kármán vortex shedding starts building up and finally saturates. During this transient, the power spectrum shows no remnant of the 560 Hz forcing frequency.

### 4.2. *Results*

First, the dependence of the saturation amplitude on Reynolds number is compared on figure 3 with the relation (3) obtained from the SL-equation, where the generic parameter $P$ is replaced by $Re$. Here and in the following, the amplitude of the global Kármán mode is characterized by the streamwise velocity oscillation at $(x/D, y/D) = (10, 1)$, unless noted otherwise. The fit of (3) to the data on figure 3 shows a close proportionality between $|A|_{sat}$ and $(Re - Re_{cr})^{\frac{1}{2}}$ and yields a value for the critical Reynolds number of $Re_{cr} = 79.2$. To verify that the forcing at around 1.8 times the natural shedding frequency does lead to a globally stable wake, the saturation amplitude has been investigated as a function of forcing amplitude $A_f$ at three fixed supercritical Reynolds numbers, where $A_f$ is measured at the centre span using stroboscopic illumination and a telescope. The results in figure 4 again show the square-root dependence (3) of $|A|_{sat}$ on the control parameter, in this case $(A_f - A_{f,cr})$, which is indicative of a Hopf bifurcation. In addition we find from figure 4 the critical forcing amplitude as $(A_{f,cr}/D) \simeq 0.008(Re - Re_{cr})$. With this we have demonstrated that the forcing has a stabilizing effect on the global Kármán mode.

The study of saturation amplitudes does, however, not allow the determination of individual constants of the SL-equation. For this purpose, transient experiments have

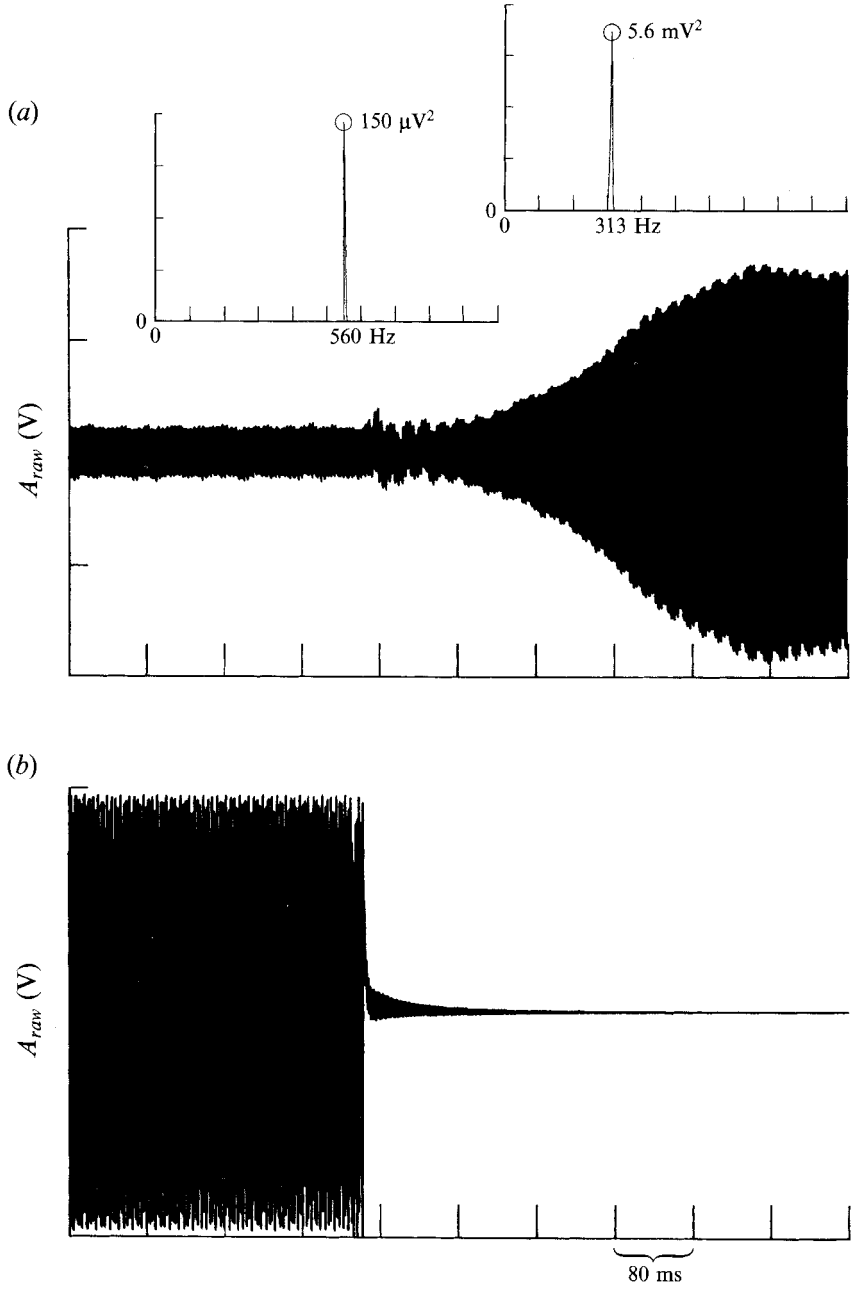


FIGURE 2. (*a*) Raw hot-wire record of supercritical transient at $(x/D, y/D) = (10, 1)$ for the oblong cylinder at $Re = 83$ with power spectra of the suppressed and the saturated state (linear scale). (*b*) Corresponding voltage across the cylinder electrodes.

been carried out. They are typified by figures 5 and 6, which correspond to supercritical and subcritical Reynolds numbers, respectively. Figures 5(*a*) and 6(*a*) show the raw transients, while the (*b*) and (*c*) parts represent instantaneous growth rate $\sigma_r$ and frequency $\sigma_i/2\pi$ plotted versus instantaneous amplitude squared, as suggested by the SL-model of §2.

The supercritical transient of figure 5 clearly illustrates the contamination by noise

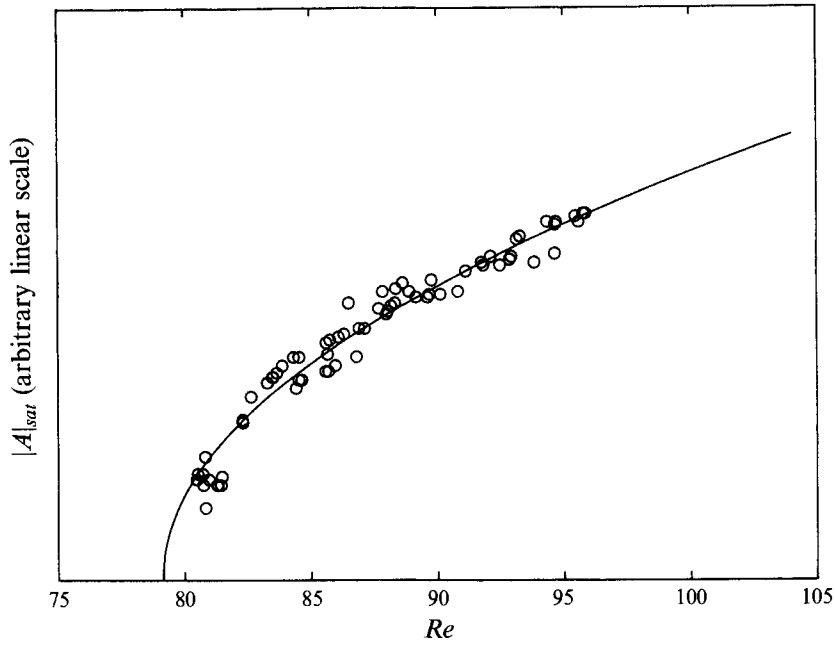


FIGURE 3. Saturation amplitude at $(x/D, y/D) = (10, 1)$ behind the oblong cylinder versus Reynolds number.

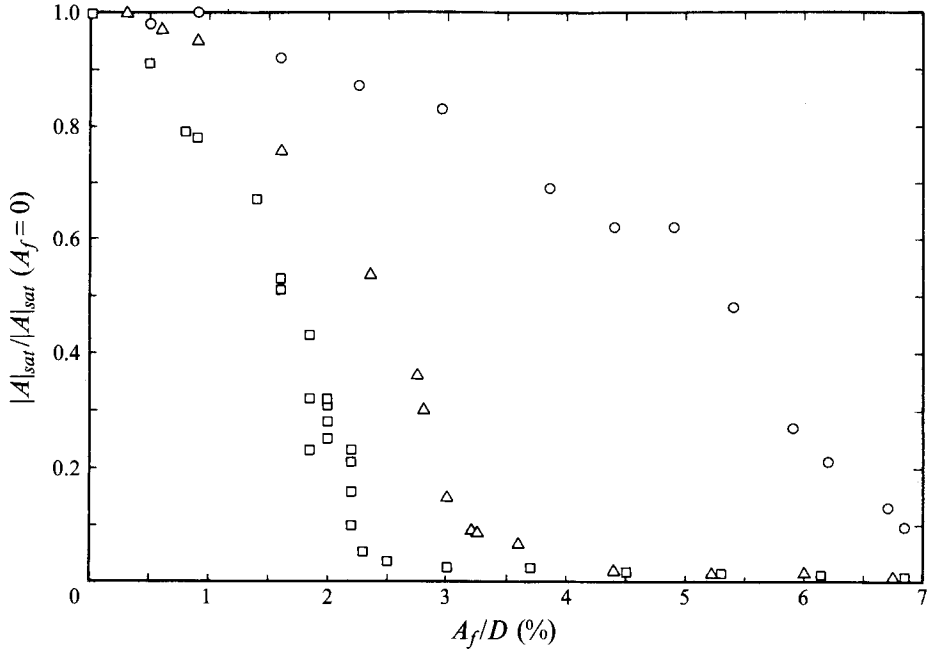


FIGURE 4. Saturation amplitude at $(x/D, y/D) = (10, 1)$ behind the oblong cylinder versus amplitude of transverse cylinder oscillation at 1.8 times the natural shedding frequency. □, $Re = 81.5$, △, $Re = 83$; ○, $Re = 89.5$.

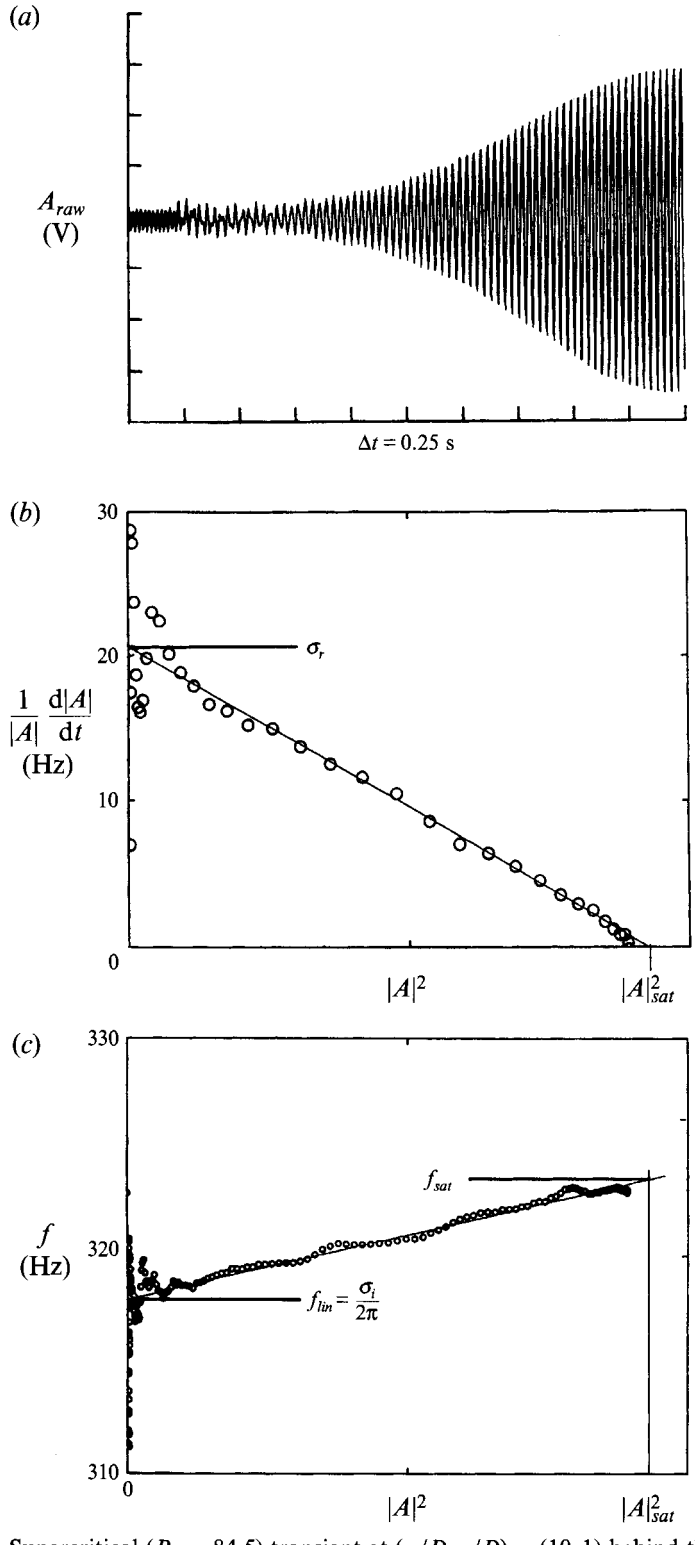


FIGURE 5. Supercritical ($Re = 84.5$) transient at $(x/D, y/D) = (10, 1)$ behind the oblong cylinder. (*a*) Raw transient. (*b*) Instantaneous growth rate versus $|A|^2$ fitted by equation (4*a*). (*c*) Instantaneous frequency versus $|A|^2$ fitted by equation (4*b*).

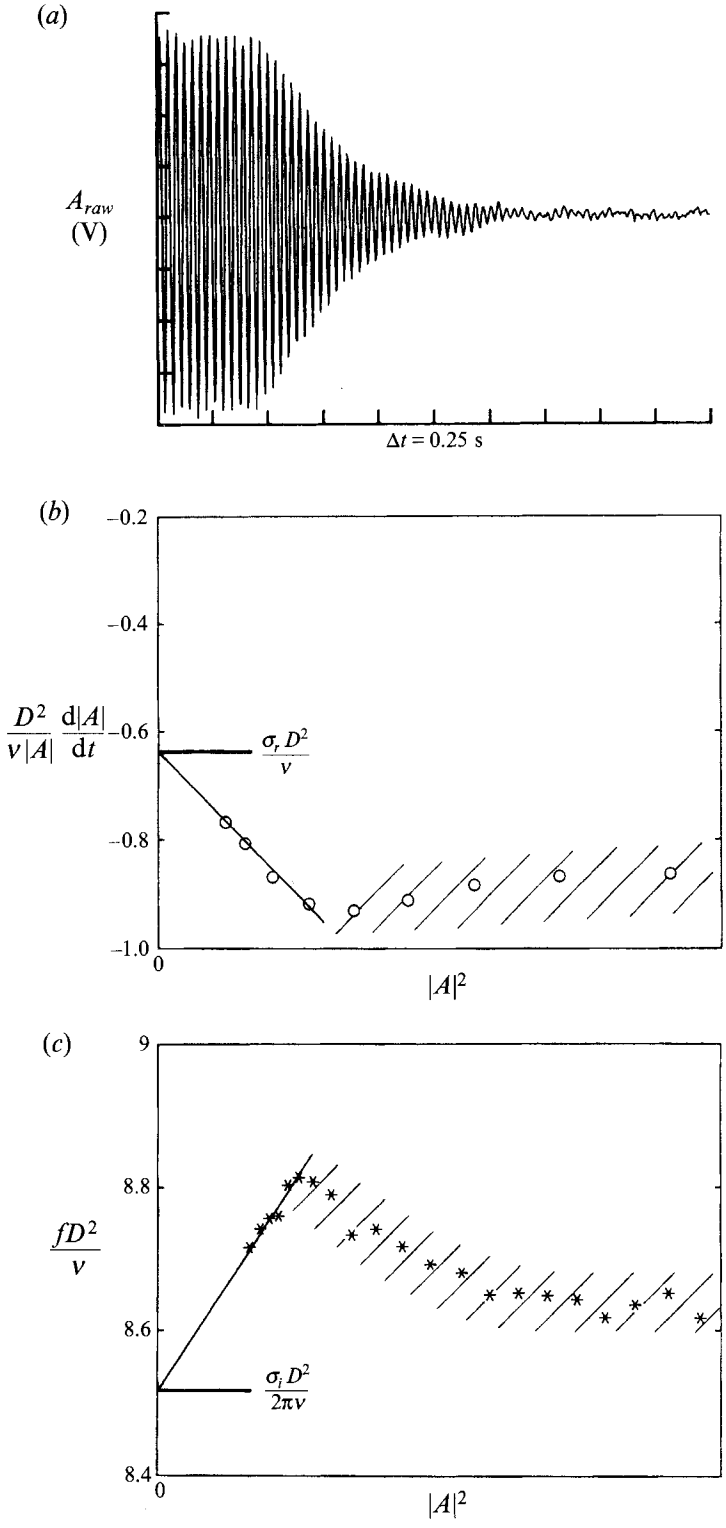


FIGURE 6. Subcritical ($Re = 74$) transient at $(x/D, y/D) = (10, 1)$ behind the oblong cylinder. (*a*) Raw transient; (*b*) instantaneous growth rate versus $|A|^2$ fitted by equation (4*a*). (*c*) Instantaneous frequency versus $|A|^2$ fitted by equation (4*b*).

at low amplitude and shows the improvement of $\sigma_r$ and $\sigma_i$ obtained by extrapolating the linear relationships (4*a*) and (4*b*) from intermediate to zero amplitudes. Figure 5(*c*) furthermore shows how easily the difference between saturation frequency $f_{sat}$ and linear frequency $\sigma_i/2\pi$ is determined which is, according to (4*b*), equal to $-(\sigma_r l_i/l_r)/2\pi$ and yields the normalized Landau constant.

To produce a decaying transient like the one of figure 6 at the subcritical Reynolds number of $Re = 74$, one has to start from a state of forced vortex shedding. This immediately raises the question of the 'correct' forcing frequency which is, in the case of the piezoceramic cylinder, freely adjustable. From the stability ideas of §2 it is seen that one has to choose the frequency which yields the minimum linear decay rate. In practice it has often been sufficient to take the slope $[\mathrm{d}\sigma_i/\mathrm{d}(Re)](Re_{cr})$ determined at supercritical Reynolds numbers and to force at the frequency obtained by extrapolating $\sigma_i$ to $Re < Re_{cr}$. Once the question of frequency is settled the decaying transient is again analysed according to the relations (4) by looking for a range of proportionality between instantaneous growth rate or frequency and $|A|^2$. Considering the typical example of figure 6 one realized immediately that this procedure is the only reliable way to interpret subcritical transients and, in particular, to separate the undesirable switch-off transient of the control from the hydrodynamic transient of interest. This is illustrated on figure 6(*b*) where the (linear) mechanical cylinder oscillations appear to decay at a rate around 0.9 and contaminate the data identified by hatching. After the noisy data at small amplitudes are also eliminated (left off the graph), only a small proportionality range for the extrapolation of $\sigma_r$ and $\sigma_i$ is left. The same is true for the frequency on figure 6(*c*), where we note in addition that the initial forcing frequency should have been chosen somewhat higher in order to be compatible with the forcing amplitude, i.e. to avoid the initial rise in frequency.

Transient experiments of the type shown on figures 5 and 6 have been carried out at many different Reynolds numbers between 73 and 97. The results for the normalized linear growth rate $\sigma_r(Re)$ are compiled on figure 7. Figure 7(*a*) shows the linear global growth rates obtained by extrapolating to zero amplitude as described above. On figure 7(*a*) the linear relationship (2*b*) has been fitted individually to the subcritical and supercritical data to demonstrate that the two regressions are essentially identical. This allows a determination of the critical Reynolds number and $\sigma_r(Re)$ with high precision

$$Re_{cr} = 79.2 \pm 0.2, \tag{6a}$$

$$\sigma_r D^2/\nu = [0.116 \pm 0.002](Re - Re_{cr}). \tag{6b}$$

For comparison, the data have also been reduced without the help of our extrapolation technique. In this case the raw transients were displayed on a semi-logarithmic scale and the slope of the straight-looking part of the envelope was taken to be "$\sigma_r$". The results of this ad hoc procedure are shown on figure 7(*b*) and clearly reveal a problem near $Re_{cr}$: with the supercritical data one obtains $Re_{cr} \simeq 78.5$, while the subcritical data yield $Re_{cr} \simeq 81$. This is easily understood with the relation (4*a*); as supercritical transients typically 'look best' at intermediate amplitudes where $|A|/|A|_{sat} \approx \frac{1}{2}$, the growth rate is underpredicted by 25%. This corresponds to a slope $[\mathrm{d}''\sigma_r''/\mathrm{d}(Re)]$ on the supercritical side of figure 7(*b*) which is only 75% of the true slope on figure 7(*a*). For the subcritical data, on the other hand, one observes the correct slope but a shift to higher damping. This is due to the fact that in our case all data points were obtained with a fixed initial forcing amplitude. If the slope is again evaluated at a fixed fraction of the initial amplitude, the relation (4*a*) indeed predicts a fixed reduction of growth rate by $l_r|A|^2$.

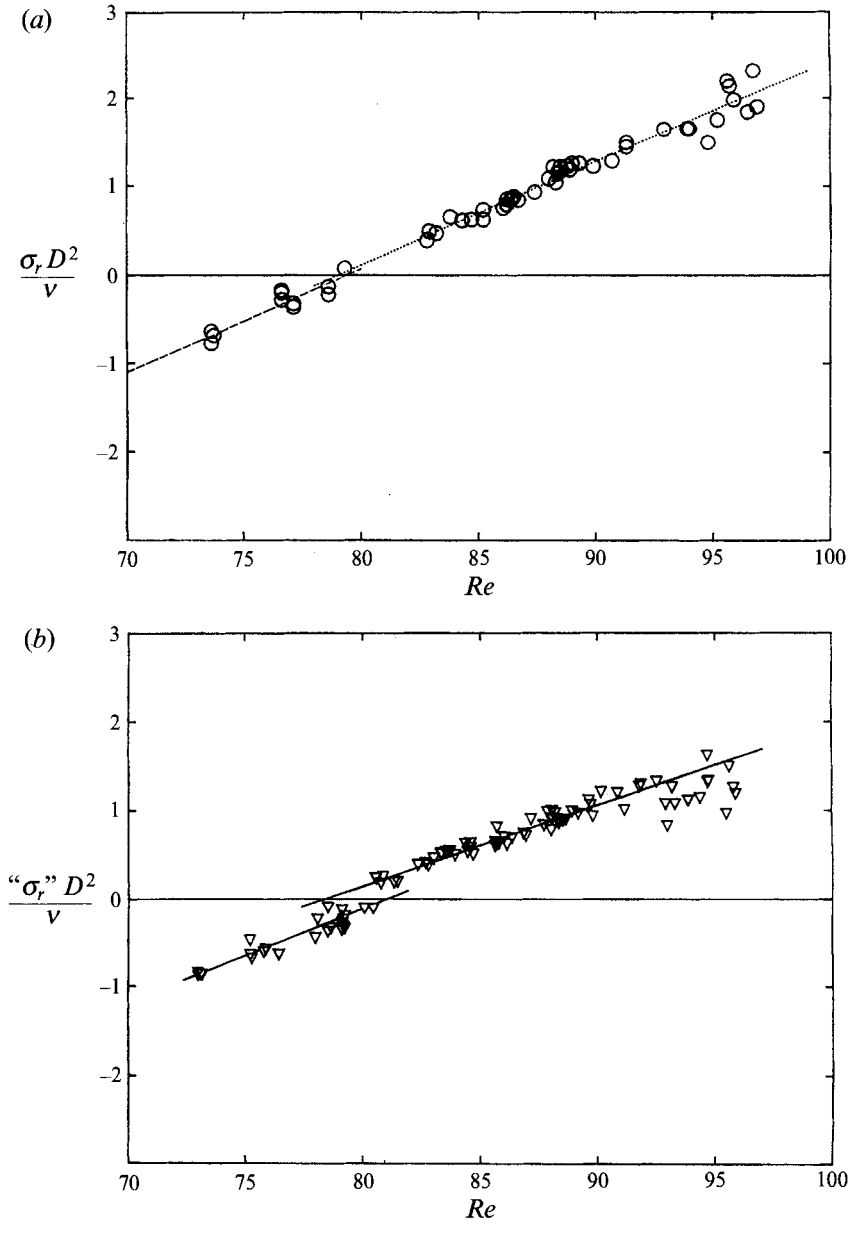


FIGURE 7. Linear global growth rate for the oblong cylinder versus Reynolds number, with equation (2*b*) fitted to the data: (*a*) $\sigma_r$ obtained by extrapolation to zero amplitude. (*b*) "$\sigma_r$" determined in the conventional manner at finite amplitude.

Analogous to the linear growth rates of figure 7(*a*), we obtain the linear frequency by extrapolation of the instantaneous frequency to zero amplitude and the normalized Landau constant from the difference between saturation frequency and linear frequency. The results are displayed on figures 8 and 9, respectively, from which we obtain

$$\sigma_i D^2/\nu = [58.1 \pm 0.3] + [0.84 \pm 0.01](Re - Re_{cr}), \tag{6c}$$

$$l_i/l_r = -[1.85 \pm 0.35]. \tag{6d}$$

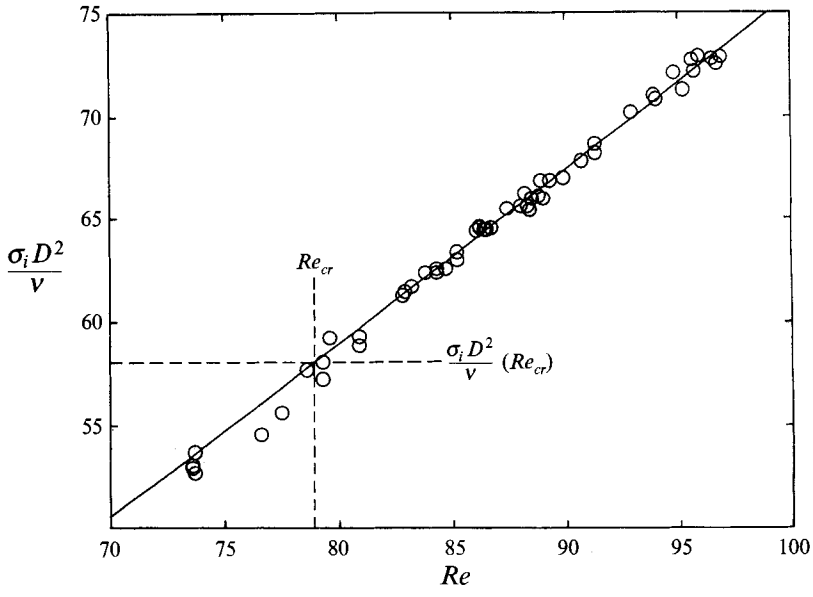


FIGURE 8. Linear frequency for the oblong cylinder versus Reynolds number, with equation (2*b*) fitted to the data.

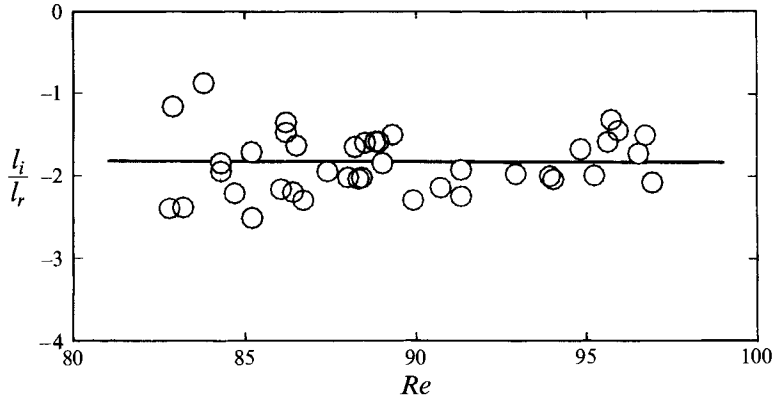


FIGURE 9. Normalized Landau constant $l_i/l_r$ for the oblong cylinder versus Reynolds number.

We observe that the linear relationship (*b*) between $\sigma_i$ and $Re$ is again followed by the data of figure 8 to a high degree of accuracy and that the Landau constant is indeed a constant, i.e. does not show any trend up to the highest Reynolds number $Re = 97$ we considered.

Finally, we present the first comprehensive experimental evidence for the 'two-step scenario' at supercritical conditions which stipulates that after a linear global mode is established, there is a period where it grows as a whole at the linear global growth rate $\sigma_r$ before saturation occurs. Hence the concept is verified by comparing growth rates at different spatial locations, an approach which has been taken before in the numerical experiment of Hannemann & Oertel (1989) and touched upon by Strykowski &

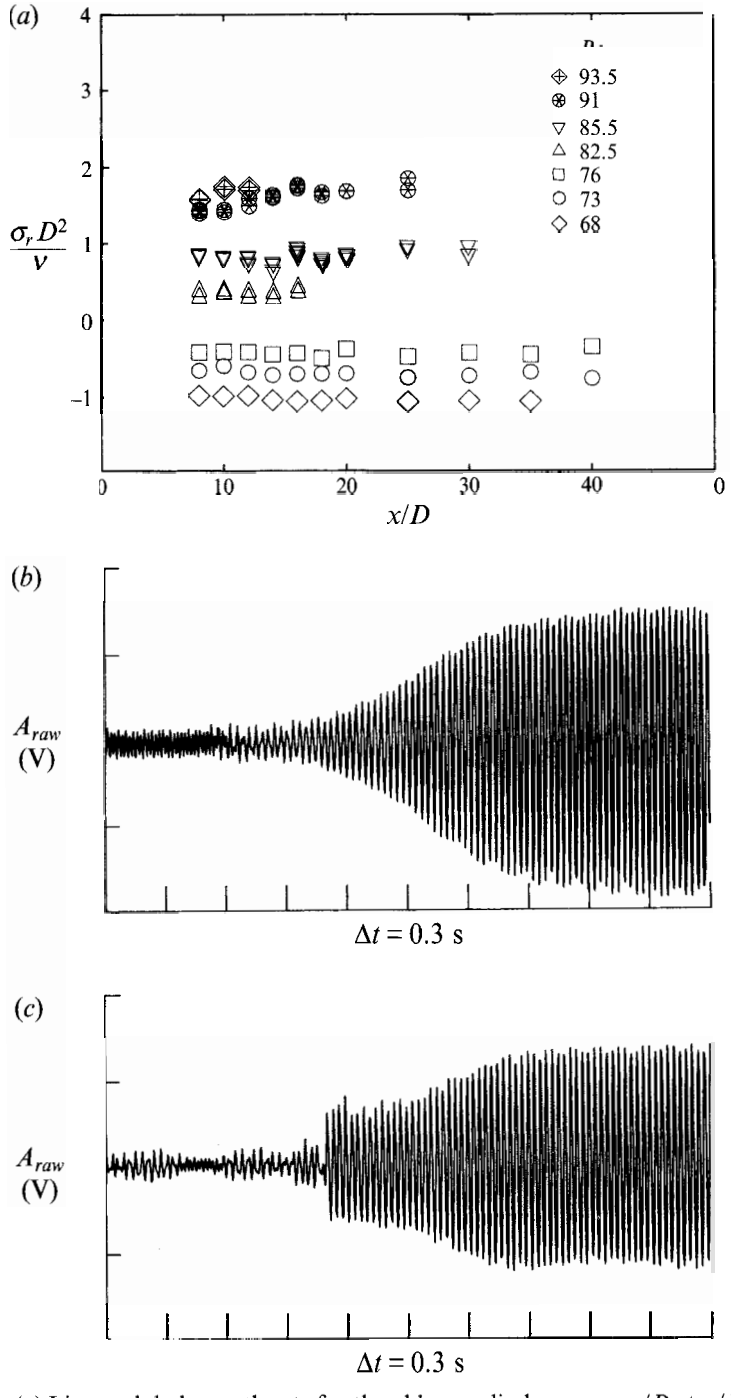


FIGURE 10. (*a*) Linear global growth rate for the oblong cylinder versus $x/D$ at $y/D = 1$ and different Reynolds numbers. (*b*) Raw transient at $x/D = 8$ for $Re = 85.5$. (*c*) Raw transient at $x/D = 30$ for $Re = 85.5$.

Sreenivasan (1990). The comparison is shown in figure 10(*a*) for seven Reynolds numbers and hot-wire locations between $(x/D, y/D) = (8, 1)$ and $(40, 1)$. We note that the probe could not be moved closer to the cylinder than $8D$ because of probe interference. The data at subcritical Reynolds numbers clearly show that the forcing excites a lightly damped global mode which decays everywhere at the same rate. At supercritical Reynolds numbers up to $Re = 85.5$, $\sigma_r$ is also found to be constant all the way to $x/D = 30$. The same holds true for different transverse locations between $0.5D$ and $2.5D$ at $x/D = 10$ (Schumm 1991). There are, however, limitations to the model which manifest themselves far downstream: in the near wake at $x/D = 8$ (figure 10*b*) the vortex shedding always starts building up immediately after the forcing is turned off, but at $x/D = 30$ (figure 10*c*) it takes the linear global mode much longer to form from the initial disturbance. As a consequence the time during which the global mode grows as a whole is shortened to the point where it is no longer possible to extrapolate a linear growth rate $\sigma_r$. As the transients grow ever shorter at $Re = 91$ and 93.5, the problem is aggravated and the last reliable data point on figure 10(*a*) moves upstream.

## 5. The wake of a circular cylinder: control by wake heating, base bleed and forced transverse oscillations

### 5.1. *Experimental set-up*

All the experiments with circular cylinders were carried out in the same facility as those with the oblong cylinder, except that it was fitted with a rectangular contraction of $160 \times 200$ mm instead of the round nozzle and a rectangular test section of 600 mm length. All cylinders tested in this set-up had a length $L = 200$ mm.

The wake heating for $Re > 57$ was effected by one or two constantan wires stretched parallel to the cylinder and close to its surface near the rear stagnation point, i.e. in the recirculation region. In each case it was verified that the unheated wires with diameters between 2% and 10% of $D$ had no influence on the natural vortex shedding. In other words, the control cylinder effect of Strykowski & Sreenivasan (1990) was avoided. Below $Re = 57$, $D$ became so small that it was no longer possible to mount a separate heating wire and the constantan wire itself served as cylinder. The temperature of the recirculation region behind the larger cylinders was measured directly with a small platinum thermometer, while in the case of the smaller cylinders it was estimated from the known relation between wire temperature and measured wire resistance. The state of the wake was in all cases monitored by a hot wire positioned at a location where there were no temperature variations.

Transverse oscillations of the cylinder were excited by two speaker coils connected to each of its ends. The tension of the cylinder ($D = 1$ mm) was adjusted to tune the mechanical resonance frequency to the excitation frequency of 1.8 times the natural shedding frequency, as in the case of the oblong cylinder. The damping of the cylinder, however, remained a problem as the best foam rubber damper could not reduce the time constant below 250 ms. Hence the transient experiments were limited to Reynolds numbers relatively close to $Re_{cr}$.

The base bleed, finally, was implemented on a cylinder of $D = 4$ mm with a slot of $h = 2$ mm, shown on figure 11. The bleed air was supplied from both ends through a central tube and a fairly uniform bleeding across the span (within 20%) was achieved by a large flow resistance between the inner tube and the cylinder. Two solenoid valves on each end were used to rapidly shut off the base bleed (see also figure 17) and the

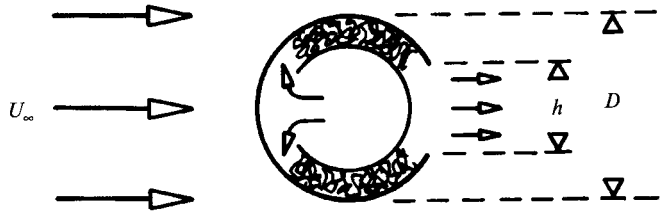


FIGURE 11. Schematic cross-section of the cylinder with base bleed with $D = 4$ mm and $h = 2$ mm.

volume flow rate $\dot{Q}$ of the bleed air was measured by a rotameter. This allowed to define the base bleed coefficient as

$$c_b = \dot{Q}/(LDU_\infty). \tag{7}$$

### 5.2. *Results*

Starting with the control by steady heating, we show on figure 12 that vortex shedding can be suppressed by this method up to at least twice the critical Reynolds number, based here on the properties of the cold free stream. Figure 12(*a*) shows the familiar bifurcation diagram for the saturation amplitude together with the non-dimensional saturation frequency. The measured temperature has been converted here to an average density $\rho_{rec}$ of the recirculation region. This was motivated by the analysis of Yu & Monkewitz (1990), but we have to point out that the temperature corresponding to $\rho_{rec}/\rho_\infty = 0.45$ is a very high $T_{rec} = 380$ °C. Hence the buoyancy driven spanwise flow must be considerable, i.e. the Richardson number $gL[1-(\rho_{rec}/\rho_\infty)]\,U_\infty^{-2}$ based on the length of the vertical cylinder is of the order of 5 and the aforementioned analysis may not be directly applicable. In figure 12(*b*) the estimated critical density ratio is plotted versus 'cold' Reynolds number. In a rescaled form this graph has been shown by Yu & Monkewitz (1990) to follow the boundary between absolute and convective instability of the most unstable profile, confirming the theoretical ideas of §2, but again, the effect of the likely spanwise thermal convection is unknown.

Next, we show the effect of base bleed and base suction on figure 13. Since the use of suction to destabilize the wake is new, the bifurcation diagrams, i.e. the saturation amplitude versus suction rate (negative bleeding rate), is presented in figure 13(*a*) for the critical Reynolds number $Re_{cr} \approx 47$ and three subcritical Reynolds numbers. We note here that a wake destabilized by suction automatically selects its natural frequency which is an advantage of suction over harmonic forcing. All the critical bleed rates are compiled on figure 13(*b*) as a function of Reynolds number. Towards larger Reynolds numbers, the bleed coefficient asymptotes toward a value $c_{b,cr}^{\infty} \approx 12\,\%$ which is in good agreement with the value for the rectangular plate at higher Reynolds number, discussed in the following section. It is also consistent with Monkewitz & Nguyen's (1987) result that typical inviscid wake profiles become convectively unstable at a bleed coefficient of 9 %. On the other side, we find that below $Re \approx 27$ it is no longer possible to induce self-excited oscillations in the wake by suction. This is consistent with the observation of Prandtl & Tietjens (1929) that the pair of recirculation vortices shows no antisymmetric oscillations below $Re = 20$, and the observations of Berger (1964) and Nishioka & Sato (1978), that no stable vortex streets could be excited below Reynolds numbers of around 20 to 25. We must conclude that around $Re \approx 27$ the suction has to be so strong that the global mode damping due to non-parallel effects overcomes the destabilizing effect of increased reverse flow.

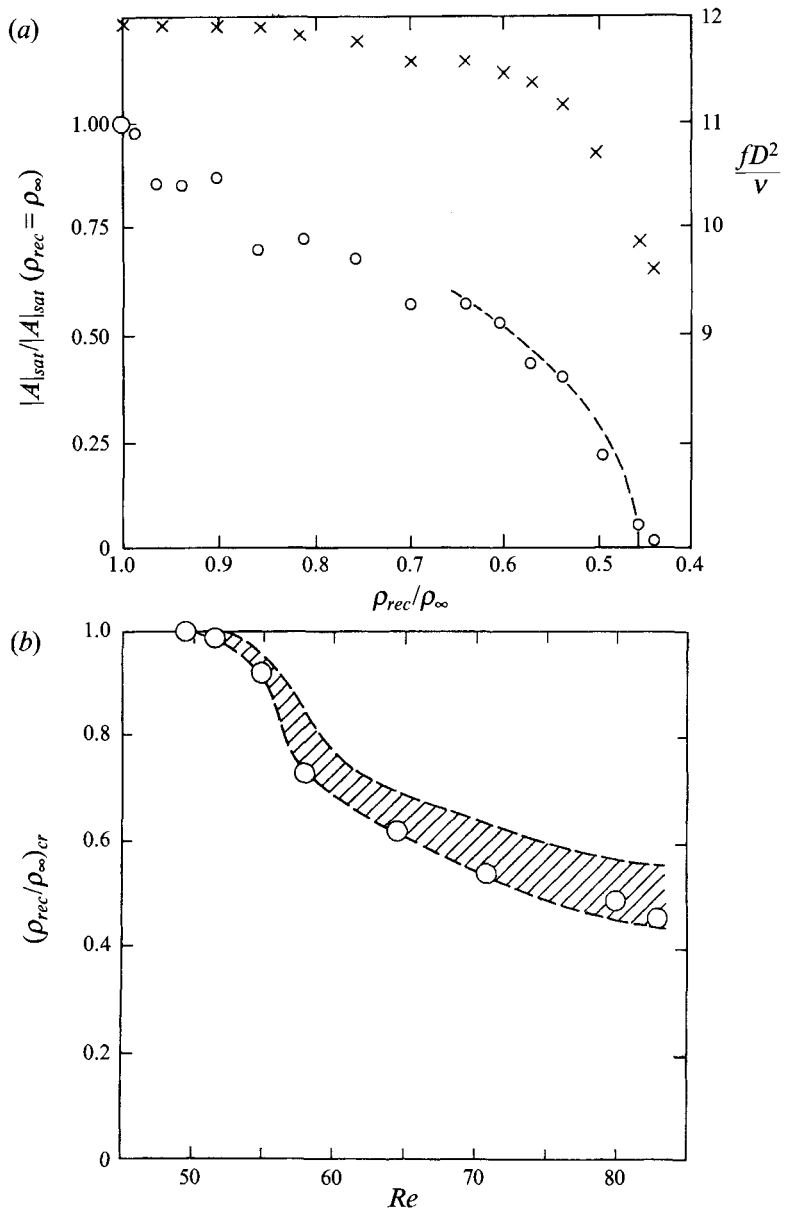


FIGURE 12. (*a*) ○, saturation amplitude and ×, frequency at $(x/D, y/D) = (8, 4)$ behind the circular cylinder versus the estimated density $\rho_{rec}$ of the recirculation zone for $Re = 83$. (*b*) Critical density ratio versus $Re$; the hatching indicates the estimated error.

The sudden interruption of base bleed, base suction or forced transverse cylinder oscillations at 1.8 times the natural shedding frequency are now used to produce transients. This is first shown on the smoke-wire visualizations of figures 14 and 15, where the smoke wire has been placed far upstream of the cylinder and perpendicular to it. Frame 14(*a*) demonstrates total suppression of vortex shedding with a bleed coefficient of 10% at $Re = 68$ (cf. figure 13*b*) behind the 4 mm cylinder of figure 11. After the bleed air is stopped, one obtains a good impression of the linear global mode on frame 14(*c*) before the standard streakline pattern develops which corresponds to

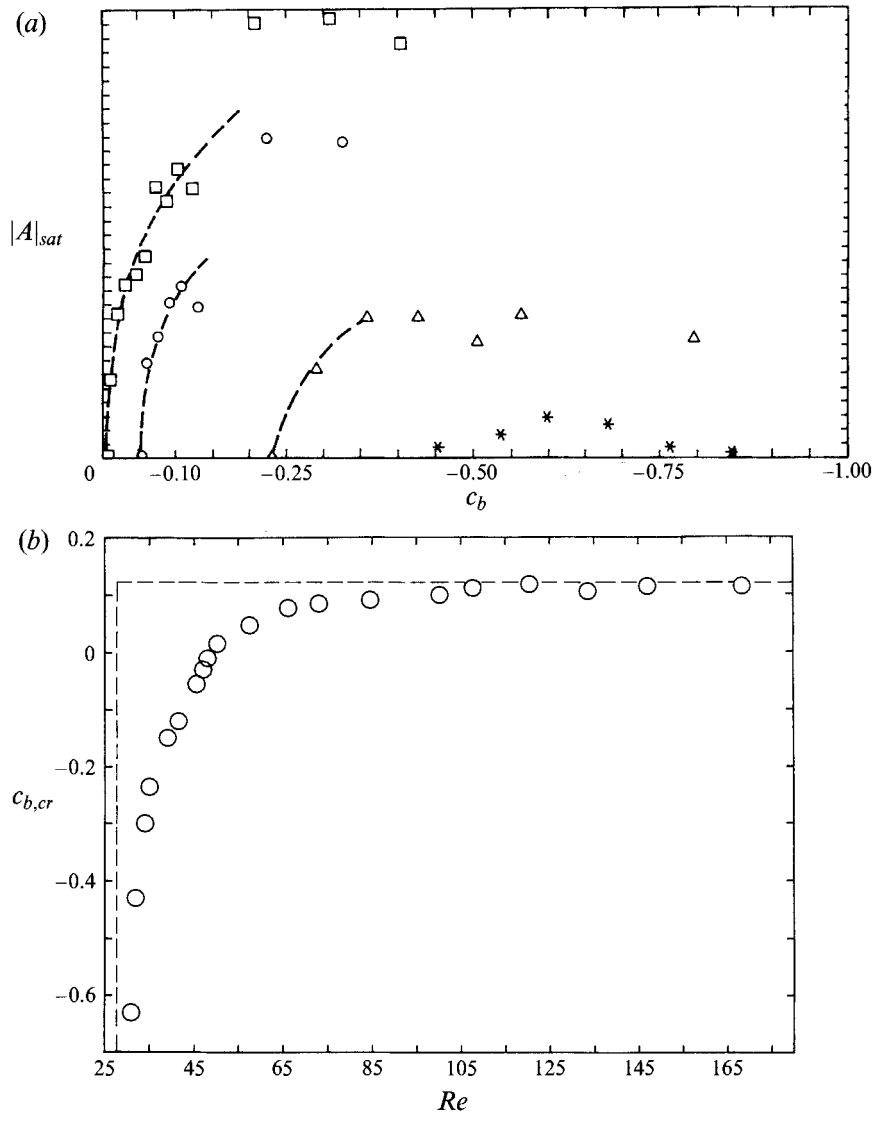


FIGURE 13. (*a*) Saturation amplitude versus base bleed coefficient for the circular cylinder at different Reynolds numbers: □, $Re = 47$; ○, $Re = 45$; △, $Re = 35$; ∗, $Re = 32$. (*b*) Critical bleed coefficient versus $Re$ with the two asymptotes indicated by broken lines.

the saturated state. Figure 15, on the other hand, demonstrates visually that transverse cylinder oscillations with a sufficient amplitude do indeed completely suppress vortex shedding (here $Re = 56$ and the amplitude on frame 15(*b*) is $0.05D$). Finally, the coefficients of the SL-equation are deduced in the same manner as for the oblong cylinder. The resulting linear growth rate, frequency and Landau constant are displayed on figure 16. Numerically we find

$$Re_{cr} = 46.7 \pm 0.3, \tag{8a}$$

$$\sigma_r D^2/\nu = [0.21 \pm 0.005](Re - Re_{cr}), \tag{8b}$$

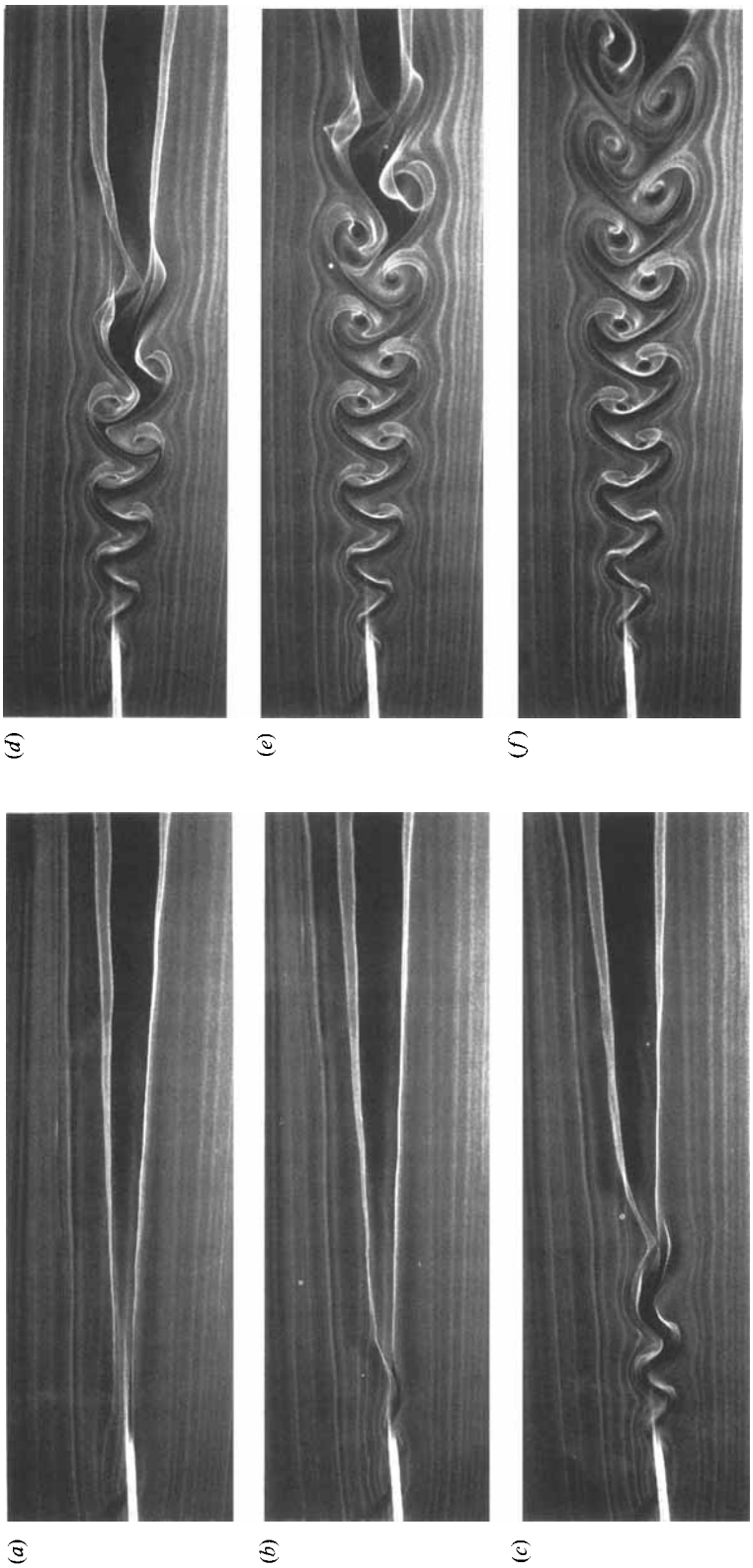


FIGURE 14. Transient in the wake of a cylinder ($D = 4$ mm, $Re = 68$) after switching off supercritical base bleed (frames are 200 ms apart). The intersection of the light sheet with the cylinder is defined by its shadow.

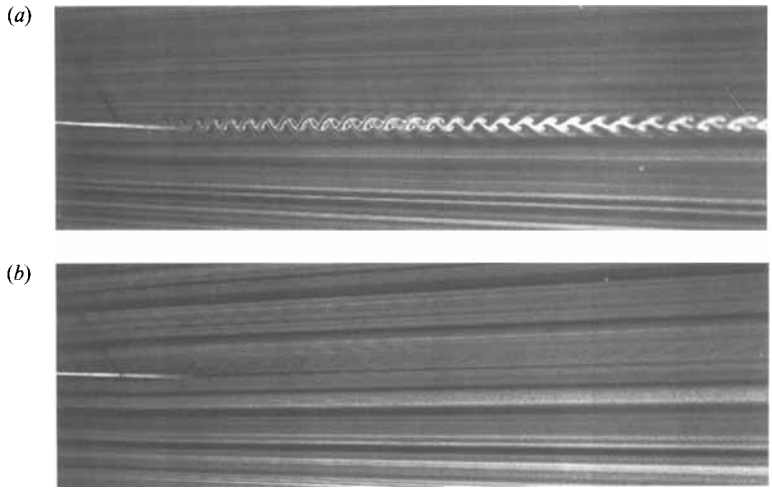


FIGURE 15. Suppression of vortex shedding behind a circular cylinder at $Re = 56$ by transverse cylinder oscillations. (*a*) No oscillations. (*b*) Oscillations at 1.8 times shedding frequency with amplitude of $0.05D$. The intersection of the light sheet with the cylinder is defined by its shadow.

$$\sigma_i D^2/\nu = [33.6 \pm 0.3] + [0.64 \pm 0.02](Re - Re_{cr}), \tag{8c}$$

$$l_i/l_r = -[2.90 \pm 0.45], \tag{8d}$$

where the data below $Re = 50$ have been discarded in figure 16(*c*). First we note that the slope of the growth rate (8*b*) is somewhat higher than the value of 0.20 published by Provansal *et al.* (1987) and Strykowski & Sreenivasan (1990). This slight increase appears owing to the fact that we have consistently extrapolated growth rates to zero amplitudes. The ratio between 0.21 and 0.20 plausibly suggests (see equation (4*a*)) that these authors have determined their growth rates, on average, at an amplitude of 22% of the saturation amplitude. We also note the excellent agreement on figure 16(*a*) between the data obtained with cylinder oscillations and with base bleed, although for historical reasons the latter technique has only been used in a few cases. This improved result for the linear growth rate is, within experimental error, identical to the value of $0.215(Re - Re_{cr})$ obtained numerically by Noack & Eckelmann (1994) and is consistent with the estimate of $\approx 0.23\ (Re - Re_{cr})$ from Morzyński & Thiele's (1993) figure 1.

The Landau constant (8*d*) is close to the value of $-3$, published by Sreenivasan *et al.* (1986), but differs somewhat from the numerical result of $-3.68$ by Noack & Eckelmann (1994), which appears difficult to reconcile with the present data. A discrepancy with the claim of Provansal *et al.* (1987) that $l_i/l_r = 0$, on the other hand, no longer exists, as their conclusion has since been revised (see the discussion in Albarède & Monkewitz 1992).

With (4*b*), results (8*a*)–(8*d*) can also be combined to yield the saturation frequency. After division by $(2\pi Re)$ we obtain the Roshko relation for the Strouhal number

$$S \equiv fD/U_\infty = -3.94/Re + 0.199. \tag{9}$$

The numerical coefficients can be compared to the values given by Williamson (1989) after his equation (6). We find that our values are closer to his three-term than his two-

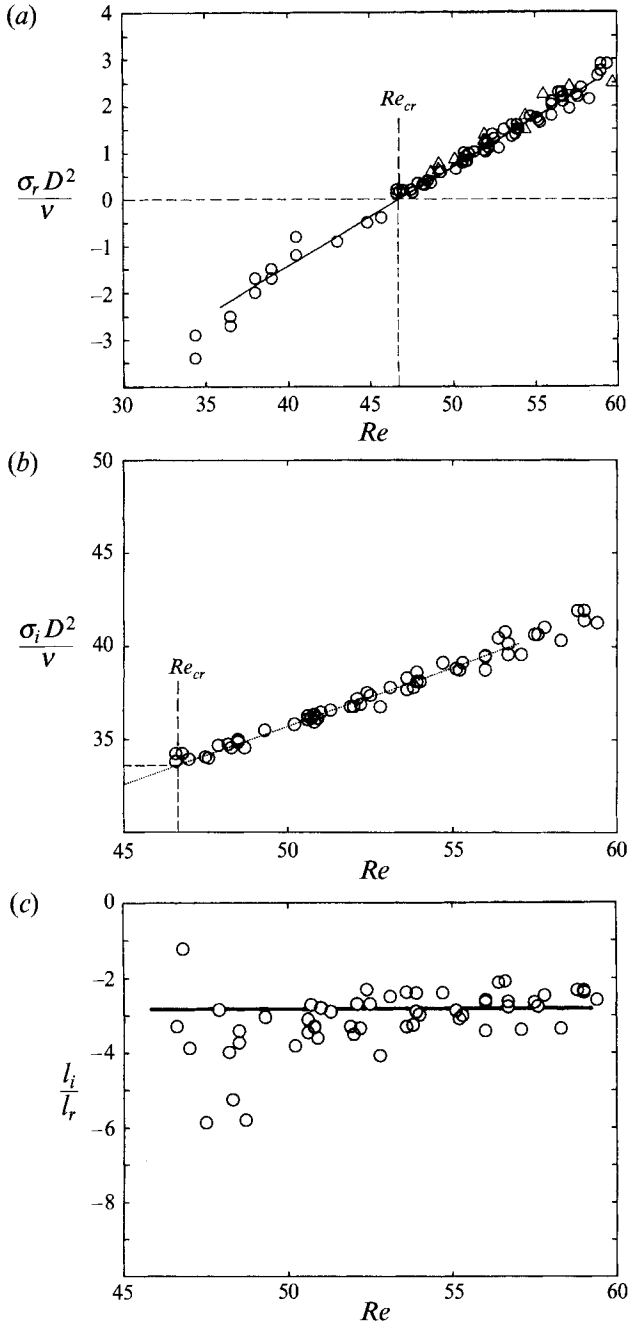


FIGURE 16. Coefficients of the Stuart–Landau equation versus $Re$ for the circular cylinder. ○, control by cylinder oscillations; △, control by base bleed.

term fit. Near the bifurcation, where the SL-equation is valid, (9) is indistinguishable from Williamson's fits, while it falls only slightly below his universal curve at $Re = 100$. This supports our contention that the transients are not contaminated by three-dimensional effects.

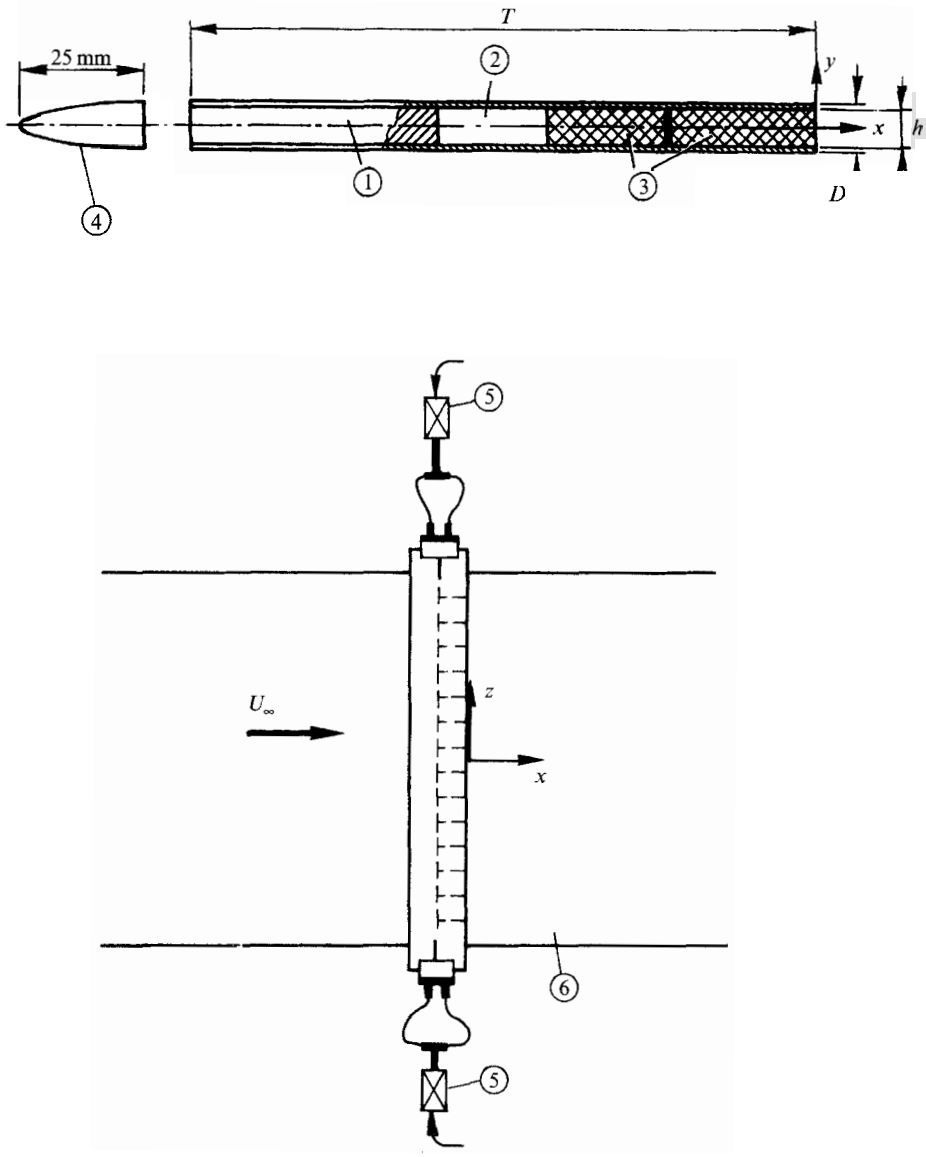


FIGURE 17. Cross-section and side view of the rectangular plates with: ① plate of $D = 4$ mm or $D = 8.6$ mm and $T/D = 15$; ② plenum for bleed air; ③ pressure drop; ④ elliptic nose for the large plate; ⑤ bleed air supply with solenoid valves; ⑥ wind tunnel test section.

## 6. The wake of blunt-based flat plates: control by base bleed

### 6.1. *Experimental set-up*

The third bluff body for this investigation was a rectangular plate with the same chord to thickness ratio $T/D = 15$ as in the numerical experiments of Hannemann & Oertel (1989). Two such models were used, a small one ($D = 4$ mm) mounted in the same facility as the circular cylinder, i.e. with a length of $L = 200$ mm, and a larger model with $D = 8.6$ mm and $L = 1400$ mm which was used for Reynolds numbers above $10^3$. The latter was mounted in the large subsonic wind tunnel of the Technical University Berlin, which has a cross-section of $1.4 \times 2$ m$^2$ and a turbulence level of 0.25%. The

plate models are shown in figure 17 with the bleed air plenum and the solenoid valves in the supply lines. Also shown is the 3:1 elliptical nose that was used on the large plate for some of the experiments. As opposed to the cylinder, the bleed slot extended in both cases essentially over the entire base of the plates.

For the acoustic forcing experiments, a woofer of 300 mm diameter was mounted at the same streamwise location as the plate trailing edge flush with one side wall of the wind tunnel test section, which had a lateral distance of 1 m from the plate. Pressure fluctuations were measured by $\frac{1}{4}$ in Bruel & Kjaer microphones (B&K 4135) with B&K 2610 amplifiers.

### 6.2. *Results*

First, the effectiveness of the base bleed on the small plate ($D = 4$ mm) is again verified by measuring the saturation amplitude at $(x/D, y/D) = (10, 1)$ as a function of bleed coefficient at different Reynolds numbers. The results are plotted on figure 18(*a*) in the form $|A|^2_{sat}(c_b)$ together with the fit (3) which allows us to extrapolate the critical bleed rates shown in figure 18(*b*). The comparison with the corresponding figure 13(*b*) for the cylinder shows that both data sets can, to a good degree of accuracy, be collapsed onto one universal curve if replotted versus the standard supercriticality parameter $(Re/Re_{cr} - 1)$.

Next, we demonstrate visually in figures 19 and 20 that the onset of vortex shedding is indeed two-dimensional as discussed in §2. The visualization is again obtained with an upstream smoke wire and the transient started from a laminar state at $Re = 200$ with a base bleed of $c_b = 0.15$. Figure 19, to be compared to figure 14, shows on the first three frames the development of a 'blip', associated with the mechanical transient of the solenoid valves, into a far-wake oscillation. Slightly after the mechanical transient the bleed stream comes to a stop and figure 19(*d*) shows a global mode concentrated in the near-wake which then develops into the steady-periodic vortex shedding. Plan views are displayed in figure 20 which are, however, not synchronized with the frames of figure 19 and represent a different transient. The first three frames of figure 20, taken at 200 ms intervals, confirm that the transient remains reasonably two-dimensional even at this relatively low aspect ratio of $L/D = 50$, while the long-time asymptotic state on figure 20(*d*) is clearly three-dimensional. In a few cases it has been verified that, after the two-dimensional saturation (typically 20 periods later for the cylinder at Reynolds numbers between 50 and 65), the frequency indeed decreased in accord with the results of Williamson (1989) and Eisenlohr & Eckelmann (1989) for oblique vortex shedding.

The results for the linear growth rate are compiled in figure 21. For historical reasons – the small plate experiment was designed to be just a preliminary test for the large plate – only the linear growth rates have been determined and this mostly by the 'old' data reduction technique in which no extrapolation to zero amplitude is carried out. Hence, the graph shows the typical discontinuity at the critical Reynolds number (cf. figure 7*b*). However, a few transients were recorded in a form amenable to the new complex demodulation and it is those which were fitted by equation (2*b*) to yield

$$Re_{cr} = 135 \pm 3, \tag{10a}$$

$$\sigma_r D^2/\nu = [0.083 \pm 0.004](Re - Re_{cr}). \tag{10b}$$

On the same graph we also show the numerical results of Hannemann & Oertel (1989) for the same plate. While their curve has a slope similar to (10*b*), it is shifted by about $\Delta Re \approx 40$ towards lower Reynolds numbers. Correspondingly, their critical Reynolds number of about 100 is much lower than our experimental $Re_{cr}$. Consistent with these

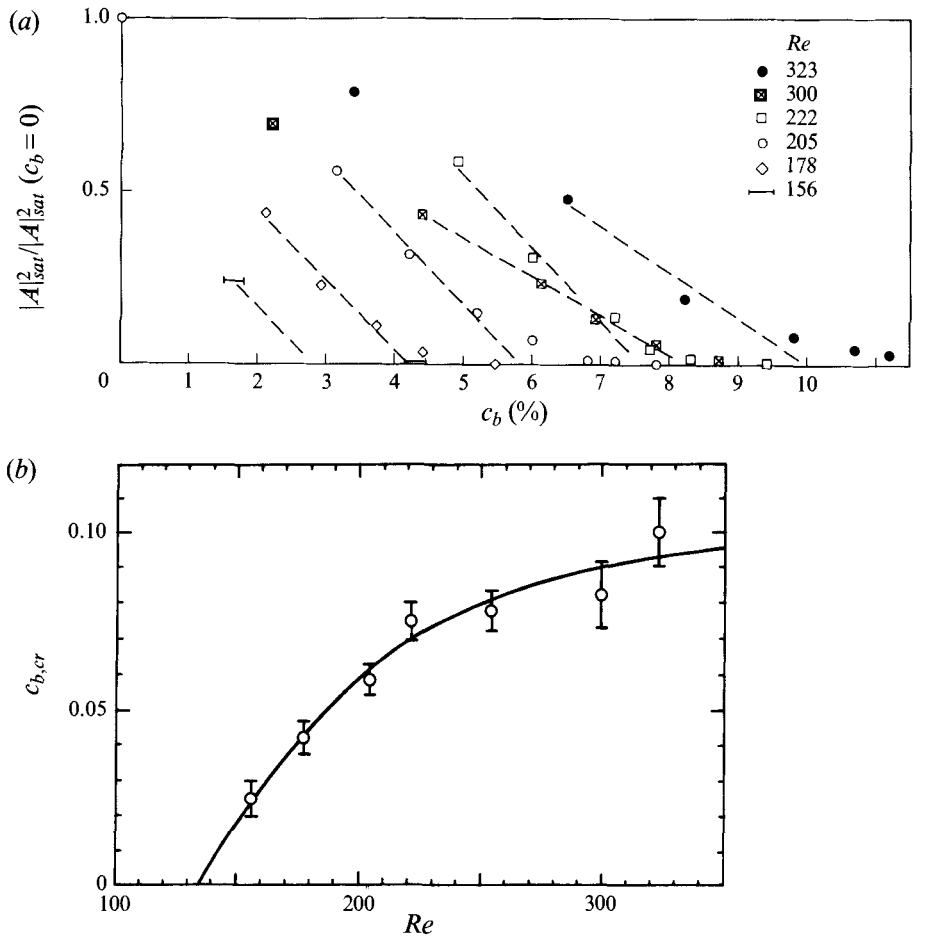


FIGURE 18. (*a*) Saturation amplitude squared versus base bleed coefficient for the small plate at $(x/D, y/D) = (4, 1)$ and different Reynolds numbers. (*b*) Critical bleed coefficient versus *Re*.

higher numerical growth rates, Hannemann & Oertel also find a critical bleed rate of $c_{b,cr} = 0.216$ at $Re = 200$ which is almost three times the experimental value of about 7% (cf. figure 18*b*). We note that the 7% are consistent with the results of Wood (1964) at higher Reynolds numbers and the stability analysis of Monkewitz & Nguyen (1987). No definite explanation for these large discrepancies can be offered, but we speculate that the strict two-dimensional nature of the computation might be responsible, since the base pressure in the experiment with finite span is certainly higher (less negative) than in the numerical simulation.

The experiments with the large plate ($D = 8.6$ mm) at Reynolds numbers between 800 and 9000 turned out to be difficult because of problems with the signal to noise (S/N) ratio. To improve the situation, the plate was fitted with an elliptic nose of 3:1 aspect ratio, shown in figure 17, which produced a laminar boundary layer at the plate trailing edge as evidenced by figure 22(*a*). For comparison the boundary layer for the square leading edge in figure 22(*b*) is clearly turbulent. The improvement of the S/N ratio is documented by the two spectra of the streamwise velocity at $(x/D, y/D) = (5.25, 1)$ shown on figure 22(*c*). Despite this modification it proved impossible to

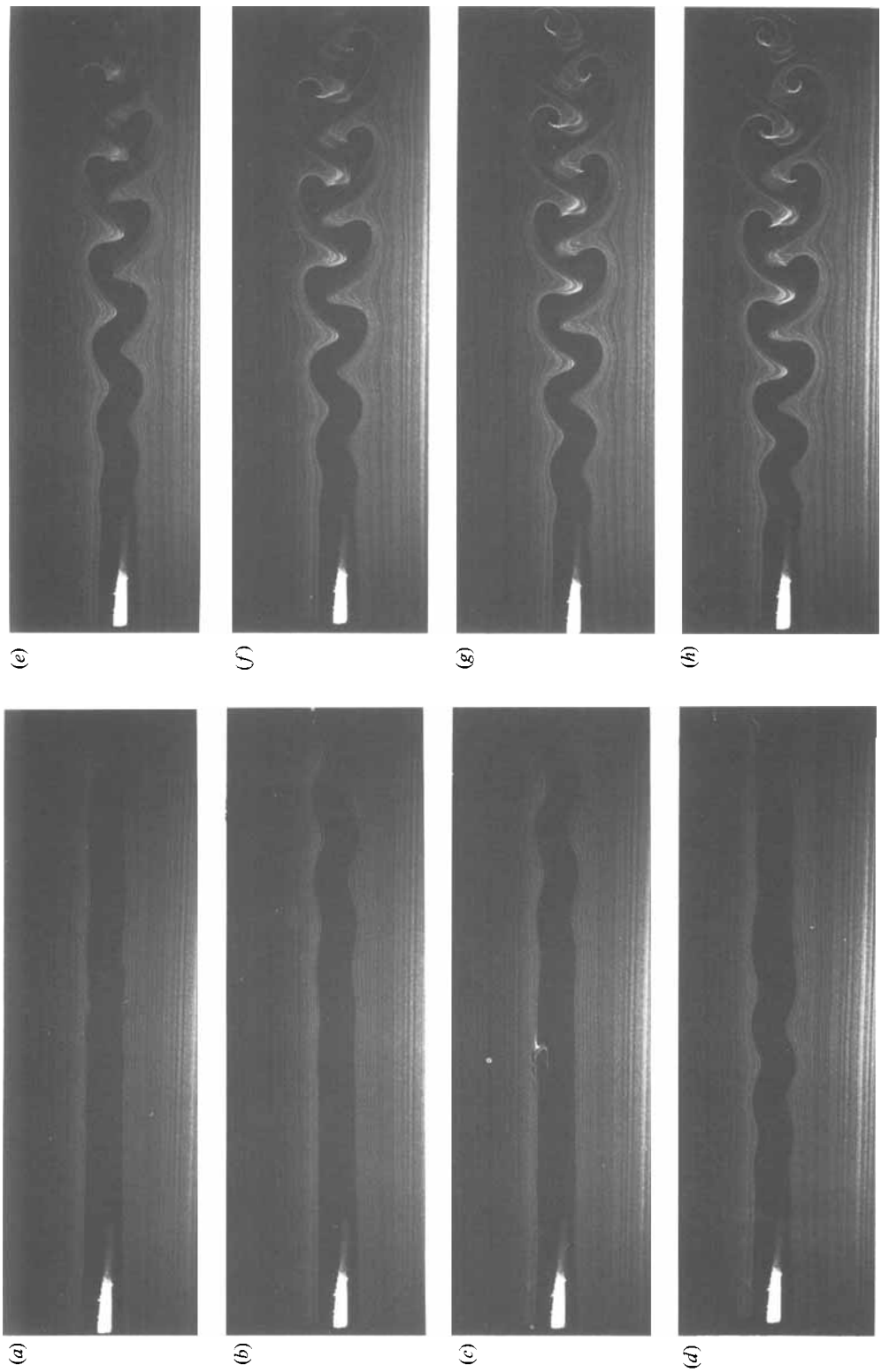


FIGURE 19. Transient in the wake of the small plate ($D = 4$ mm, $Re = 200$) after switching off supercritical base bleed (frames are 200 ms apart).

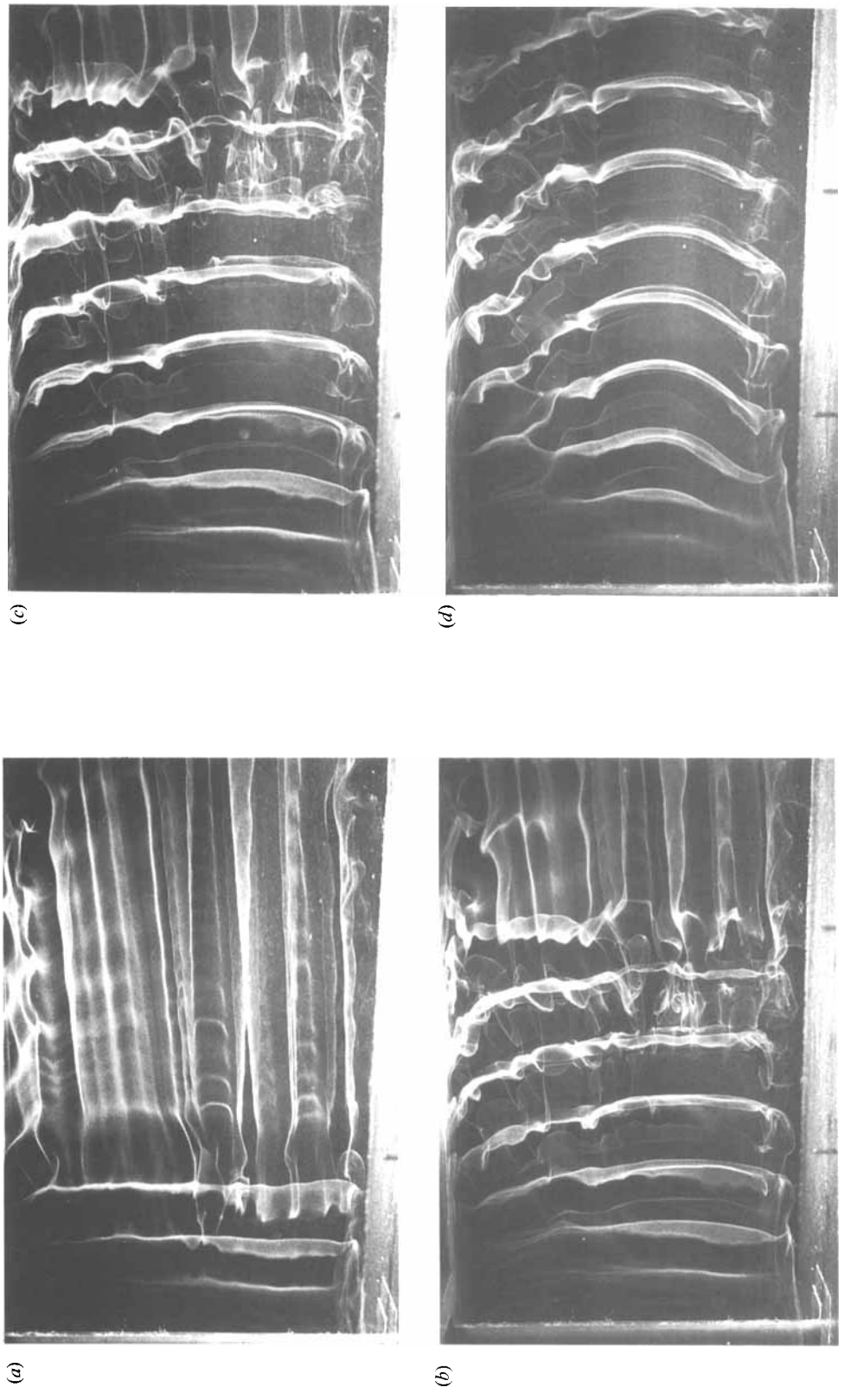


FIGURE 20. Plan view of figure 19. (*a*)–(*c*) are 200 ms apart; (*c*) corresponds approximately to saturation; (*d*) is asymptotic state with oblique shedding.

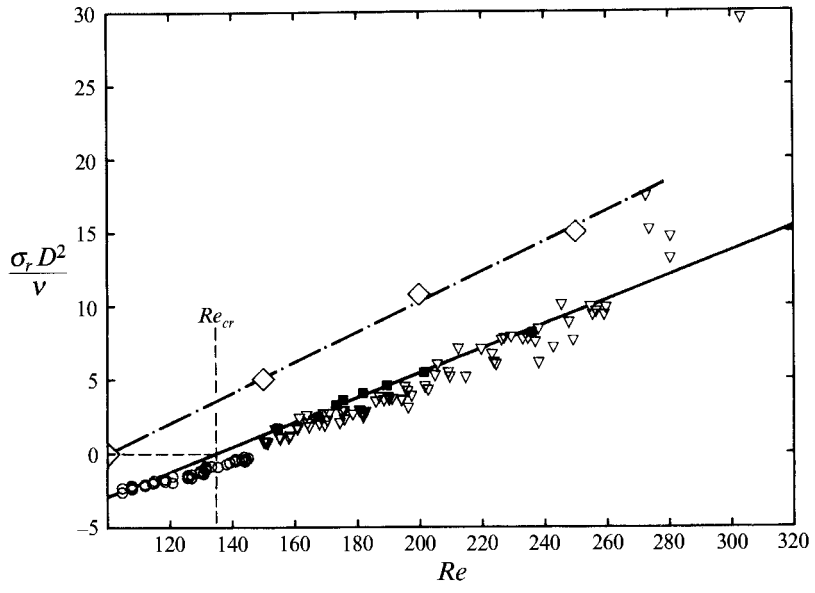


FIGURE 21. Linear growth rate versus $Re$ for the small plate. ○, ▽, transients analysed without extrapolation to zero amplitude; ■, 'true' linear growth rates; ◇, numerical results of Hannemann & Oertel (1989).

extract useful information from transients as they were too short compared to both the time it took to switch off the bleed air and the vortex shedding period. Therefore we only present results pertaining to steady limit-cycle amplitudes.

On figure 23 we show how the turbulent plate wake reacts to increasing base bleed. Up to figure 23(*d*), i.e. to 4.9% bleed, the only effect of bleed is to reduce the noise and sharpen the peak which may be interpreted as a relaminarization of the wake. Only beyond 5% bleed the amplitude of vortex shedding is progressively reduced with complete suppression at about 7%. We also note the amplitude modulation on figures 23(*e*) and 23(*f*) which is typical of wakes near the onset of vortex shedding where there is often competition between shedding at different angles. In our view this constitutes strong first evidence that the wake goes through similar stages when the bleed rate is increased at constant (turbulent) Reynolds number as when the Reynolds number is reduced to its critical value without base bleed. The state of the wake – limit-cycle or not – was further investigated by recording its response to external forcing in the manner used by Sreenivasan *et al.* (1989) in a helium jet. As in that case, we find that without base bleed the vortex shedding, characterized by the velocity at $(x/D, y/D) = (3, 1)$, does not respond to pure tone and broadband acoustic forcing up to a sound pressure level of 110 dB, as illustrated by figure 24(*a*, *b*). This strongly suggests that even at turbulent Reynolds numbers Kármán shedding remains a limit-cycle. With enough base bleed to suppress vortex shedding, on the other hand, we find a clear response as shown on figure 24(*c*, *d*) for the two types of excitation. All the forcing experiments are collected in figure 25 which strengthens our point as it shows a range of forcing amplitudes over which the response is approximately proportional to the input, which indicates that wake oscillations with supercritical base bleed are linearly damped.

Finally, the visualization of figure 26 illustrates at $Re = 850$ the differences between a suppressed state (figure 26*a*), natural vortex shedding (figure 26*d*) without base bleed

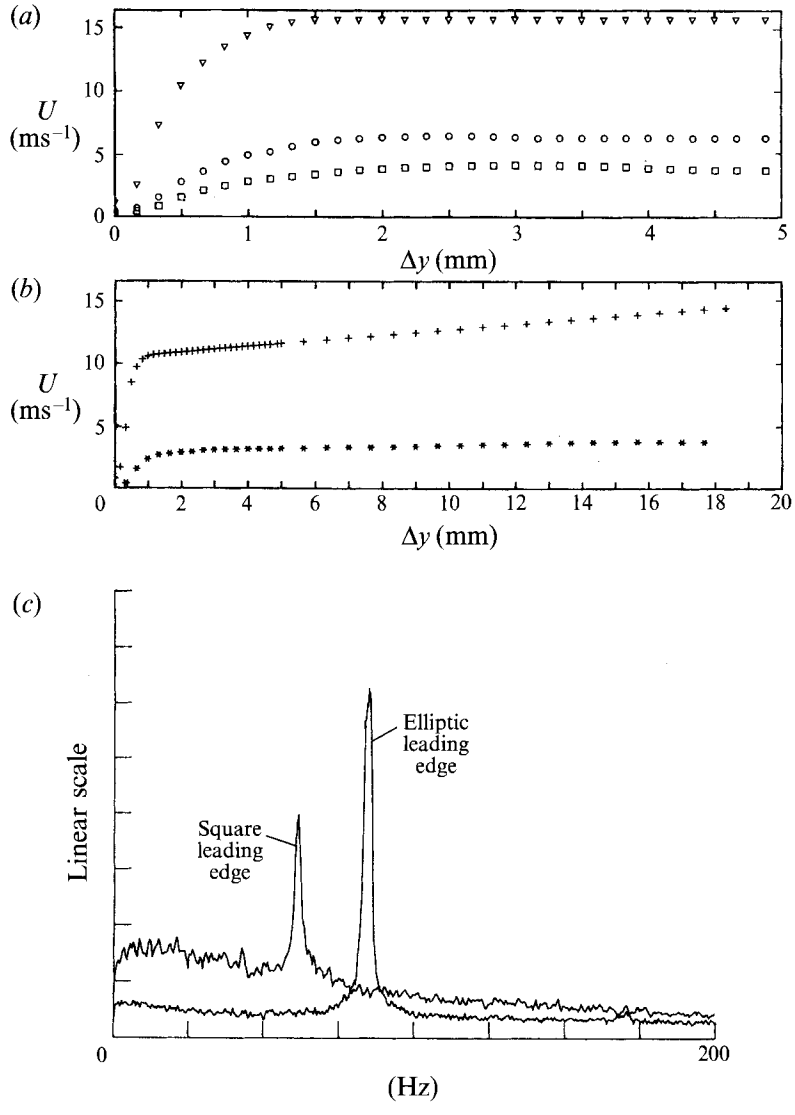


FIGURE 22. Boundary-layer profile at the trailing edge of the large plate for (*a*) elliptical leading edge ($\nabla$, $Re = 9000$; $\circ$, $Re = 3600$; $\square$, $Re = 2300$) and (*b*) square leading edge (+, $Re = 8500$; *, $Re = 2300$). (*c*) Corresponding amplitude spectra at $(x/D, y/D) = (5.25, 1)$ and $Re = 1900$.

and a suppressed state with acoustic forcing (figure 26*e*). Figure 26(*a*) clearly shows the suppression in the near wake, while the far-wake instability, which looks like Kármán shedding but is in fact a convective, noise-sustained instability, cannot be suppressed in our facility at this Reynolds number. After the base bleed is turned off, Kármán shedding starts near the trailing edge in figure 26(*b*) and then saturates very rapidly over only a few cycles. This is to be contrasted with figure 26(*e*) which shows a case with white-noise forcing at an intermediate amplitude corresponding qualitatively to figure 24(*d*).

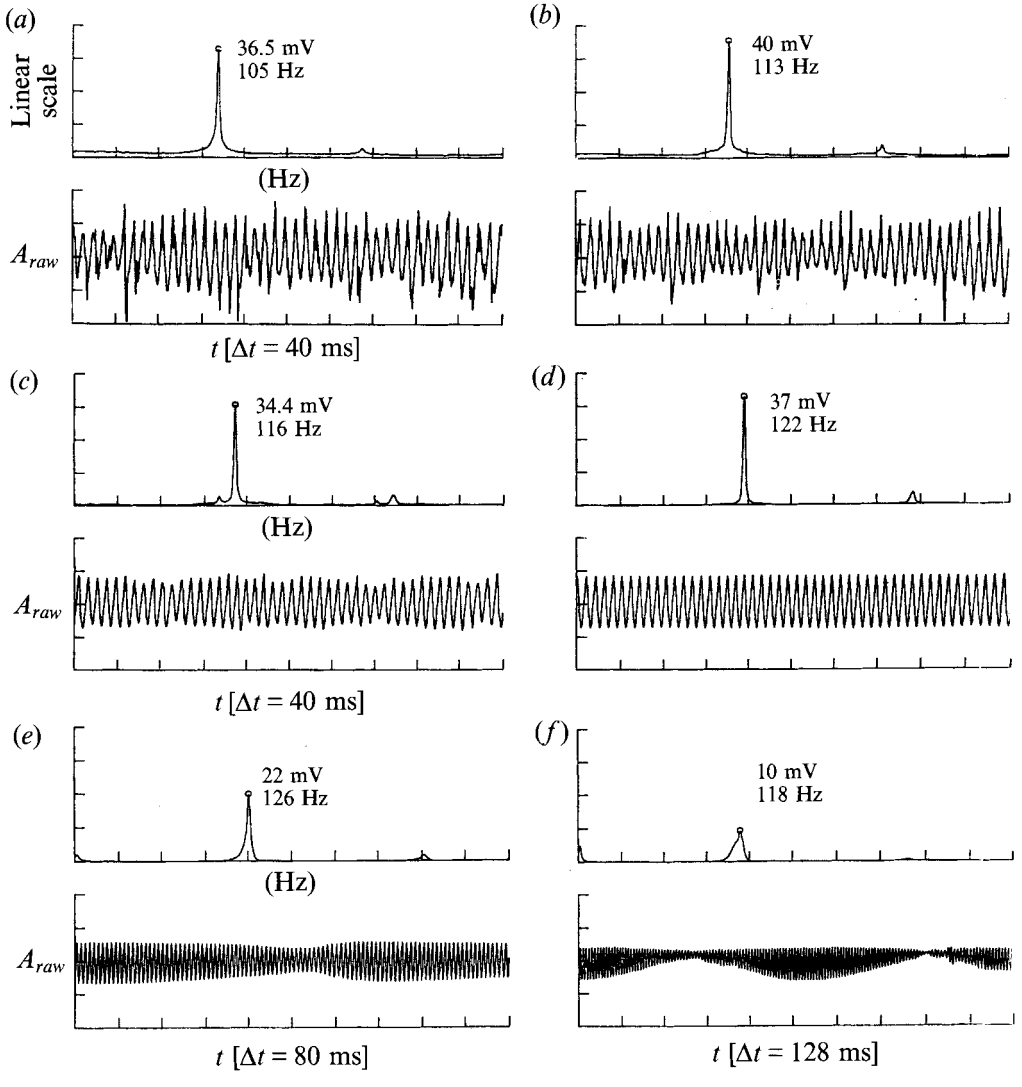


FIGURE 23. Amplitude spectra (linear scale) and corresponding hot-wire traces at $(x/D, y/D) = (3, 1)$ behind the large plate for $Re = 2300$ and varying base bleed: (*a*) $c_b = 0$; (*b*) $c_b = 2\%$; (*c*) $c_b = 4\%$; (*d*) $c_b = 4.9\%$; (*e*) $c_b = 5.2\%$; (*f*) $c_b = 6.6\%$.

## 7. Conclusions

With the present experiments we have demonstrated that the concept of weakly nonlinear global modes, which is, strictly speaking, only valid very close to the onset of vortex shedding, remains useful over a much wider parameter range. The latter extends in some cases to values of the supercriticality parameter $(P/P_{cr} - 1)$ of order unity, where $P$ is the Reynolds number, the bleed coefficient, etc. The most useful feature is thereby the possibility of characterizing the wake dynamics by a single amplitude which describes how the global Kármán mode evolves as a whole. We have presented strong evidence that this view is legitimate. In the process, we have used the technique of complex signal demodulation to make the most reliable estimates to date of the coefficients of the Stuart–Landau equation, which governs the aforementioned

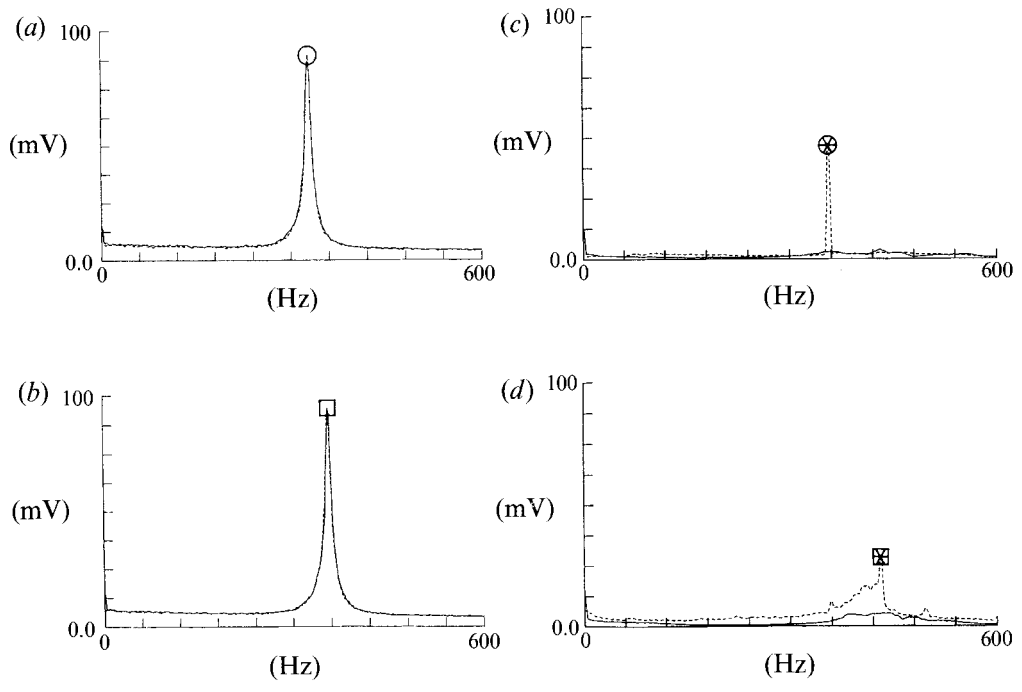


FIGURE 24. Amplitude spectra at $(x/D, y/D) = (3, 1)$ behind the large plate ——, without and – – –, with acoustic forcing. (*a*) $Re = 6600$, $c_b = 0$ and 98 dB sinusoidal forcing at $f = 357$ Hz; (*b*) $Re = 7000$, $c_b = 0$ and 84 dB white noise; (*c*) $Re = 6600$, $c_b > c_{b,cr}$ and 98 dB sinusoidal forcing at $f = 357$ Hz; (*d*) $Re = 7000$, $c_b > c_{b,cr}$ and 84 dB white noise.

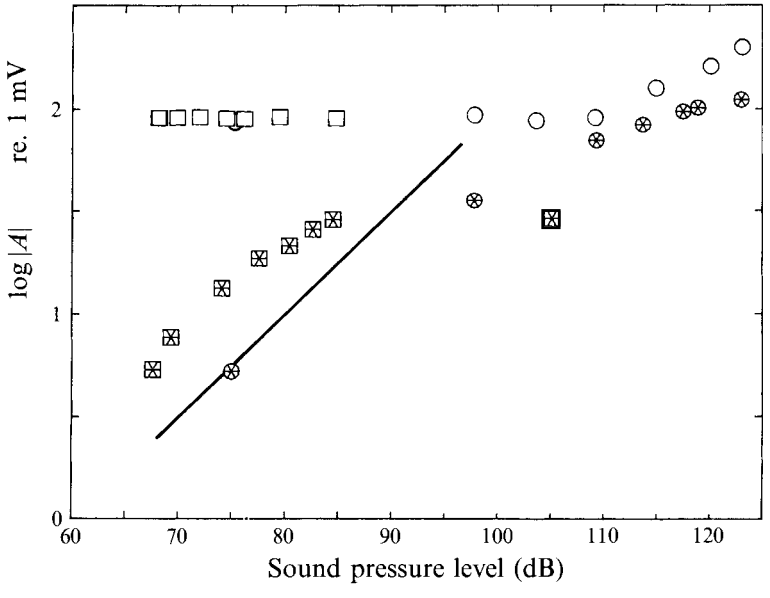


FIGURE 25. Spectral peaks of figure 24 versus sound pressure level. Symbols as in figure 24; ——, proportional relationship.

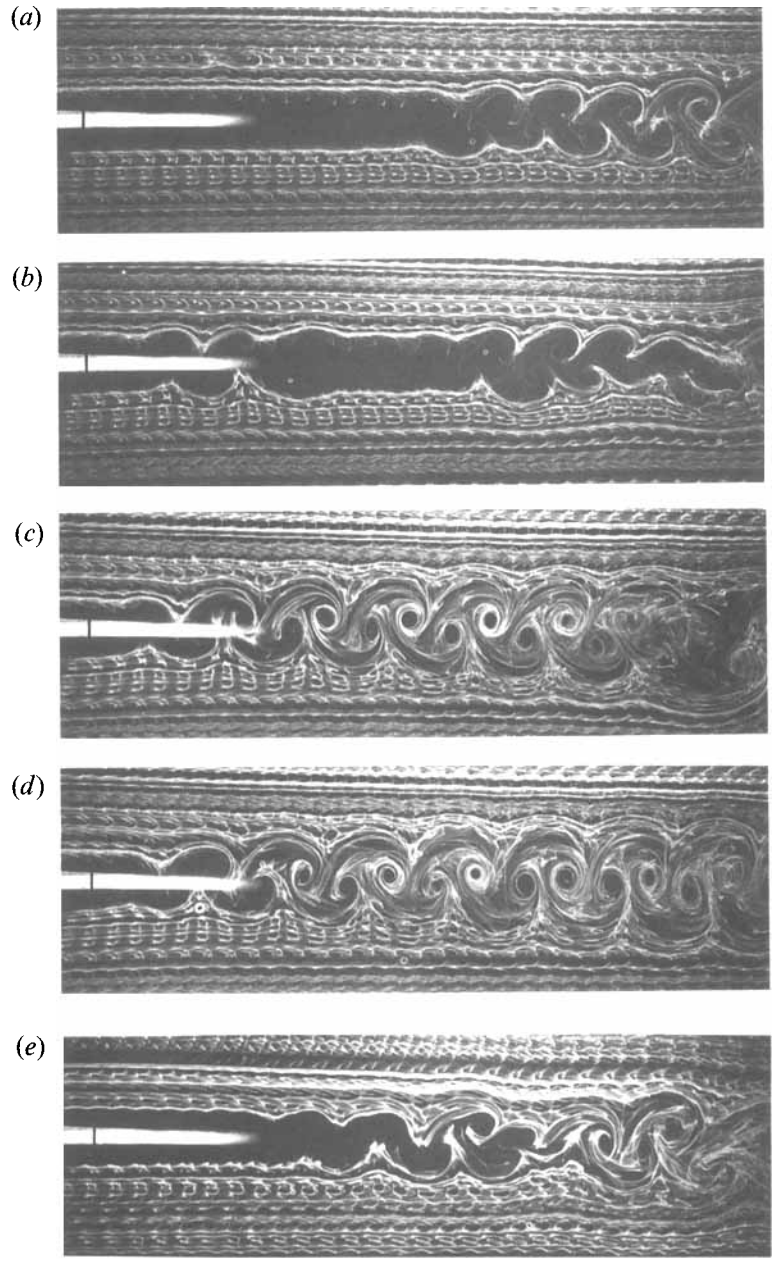


FIGURE 26. (*a*)–(*d*) Transient in the wake of the large plate ($D = 8.6$ mm, $Re = 850$) after switching off supercritical base bleed of $c_b = 20\%$ (frames are 200 ms apart). (*e*) State with $c_b = 20\%$ and acoustic forcing by white noise. The intersection of the light sheet with the plate trailing edge is marked by a black line.

characteristic amplitude in the wake of an oblong cylinder, a circular cylinder and a rectangular plate (only partial results). At the same time we have demonstrated that the experimental coefficients of the Stuart–Landau model are independent of the control technique, which is used to produce transients. Hence the Stuart–Landau model appears useful as a 'plant model' for the design of a feedback control system or

generally to predict the effect of parameter changes on vortex shedding. While these claims are strictly speaking only supported for two-dimensional symmetric bluff bodies, we point out that the Stuart–Landau model is generic to supercritical Hopf bifurcations (Stuart 1971). Hence, it should remain useful in a much larger class of wake flows, including the wakes of asymmetric two-dimensional and three-dimensional bodies (e.g. the axisymmetric body in Monkewitz 1993), as long as the flow supports unstable global modes, i.e. as long as the local absolute instability in the near-wake is not suppressed by, for instance, mean flow asymmetry.

At this point, the question naturally arises whether it is possible to also obtain our measured linear global growth rates and frequencies from the weakly non-parallel analysis of Monkewitz *et al.* (1993). Unfortunately the answer is at present negative. The third author (PAM), together with S. Le Dizès, has made a significant effort in this direction, starting from mean velocity profiles computed by Hannemann & Oertel (1989) for the wake of a plate and by Morzyński & Thiele (1993) for the cylinder wake. Despite distinct maxima of the local absolute growth rates in the recirculation region, the saddle points of the complex absolute frequency, which, according to the analysis, govern the global behaviour in doubly infinite media, were in both cases found to be too far from the real $x$-axis. As a consequence, the stability properties, which are only available on the real, physical axis downstream of the body, could not be analytically continued to the saddle point. In other words, the 'standard' wake of cylinders and rectangular plates appears to fall into a category of 'mixed' flows in which global modes are influenced by a saddle point of absolute frequency as well as the upstream boundary (the bluff body) and hence defy simple analysis. The connection between our wake experiments and weakly non-parallel theory is therefore, strictly speaking, only conceptual at present. However, there is good hope that a quantitative comparison between weakly non-parallel theory and experiments for the wake of a plate with base suction will come from C. M. Ho's laboratory at UCLA in the near future, since with sufficient base suction the local velocity profile with the largest back-flow, i.e. the most unstable profile, is located at the plate trailing edge. Therefore, the generic analysis for a semi-infinite flow domain (Monkewitz *et al.* 1993), where global modes are dominated by the 'inflow' boundary, is expected to apply. For our own experiments with base suction such a quantitative comparison was not possible for lack of highly accurate and complete mean flow data, which could only have been obtained with a non-intrusive laser doppler anemometer that was not available at the time. For this same reason we have not presented spatial distributions of oscillation amplitudes (global mode shapes) either.

For the future, one of the major challenges is to explain theoretically why these concepts of weakly nonlinear stability theory appear to be so 'unreasonably' successful in wakes that are relatively far from the primary Hopf bifurcation to Kármán vortex shedding.

P.A.M. would like to thank the Alexander von Humboldt Foundation, the DLR and the Hermann-Foettinger Institute of the Technical University in Berlin for their kind hospitality and support. P.A.M. also thanks Dr Hannemann and Dr Morzyński as well as Professors Oertel and Thiele for generously making their original data available. The financial support by the DFG under grant Be 343/18 (M.S. and E.B.) and by the US Office of Naval Research under grant N00014-90-J-1313 (P.A.M.) are gratefully acknowledged.

## REFERENCES


ALBARÈDE, P. & MONKEWITZ, P. A. 1992 A model for the formation of oblique shedding and 'chevron' patterns in cylinder wakes. *Phys. Fluids* A **4**, 744–756.

BEARMAN, P. W. 1967 The effect of base bleed on the flow behind a two-dimensional model with a blunt trailing edge. *Aero. Q.* **18**, 207–224.

BERGER, E. 1964 Unterdrueckung der laminaren Wirbelstroemung und des Turbulenzeinsatzes der Kármán'schen Wirbelstrasse im Nachlauf eines schwingenden Zylinders. *Jahrbuch der WGLR* (ed. H. Blenk), pp. 164–172. Friedr. Vieweg, Braunschweig.

BERGER, E. 1967 Suppression of vortex shedding and turbulence behind oscillating cylinders. *Phys. Fluids* **10** (Suppl.), S191–S193.

BERGER, E. & WILLE, R. 1972 Periodic flow phenomena. *Ann. Rev. Fluid Mech.* **4**, 313–340.

BRIGGS, R. J. 1964 *Electron-Stream Interaction with Plasmas.* MIT Press.

CHOMAZ, J. M., HUERRE, P. & REDEKOPP, L. G. 1988 Bifurcations to local and global modes in spatially-developing flows. *Phys. Rev. Lett.* **60**, 25–28.

CHOMAZ, J. M., HUERRE, P. & REDEKOPP, L. G. 1991 A frequency selection criterion in spatially developing flows. *Stud. Appl. Maths* **84**, 119–144.

CIMBALA, J. M., NAGIB, H. M. & ROSHKO, A. 1988 Large structure in the far wakes of two-dimensional bluff bodies. *J. Fluid Mech.* **190**, 265–298.

EISENLOHR, H. & ECKELMANN, H. 1989 Vortex splitting and its consequences in the vortex wake of cylinders at low Reynolds number. *Phys. Fluids* A **1**, 189–192.

FFOWCS WILLIAMS, J. E. & ZHAO, B. C. 1989 The active control of vortex shedding. *J. Fluids Struct.* **3**, 115–122.

GERICH, D. & ECKELMANN, H. 1982 Influence of end plates and free ends on the shedding frequency of circular cylinders. *J. Fluid Mech.* **122**, 109–121.

HAMMACHE, M. & GHARIB, M. 1991 An experimental study of the parallel and oblique vortex shedding from circular cylinders. *J. Fluid Mech.* **232**, 567–590.

HANNEMANN, K., LYNN, T. B. & STRYKOWSKI, P. J. 1986 Experimental investigation of the wake behind a flat plate with and without the influence of base bleed. *Intl Rep.* IB-221-86-A-26, DFVLR Goettingen.

HANNEMANN, K. & OERTEL, H. 1989 Numerical simulation of the absolutely and convectively unstable wake. *J. Fluid Mech.* **199**, 55–88.

HUERRE, P. & MONKEWITZ, P. A. 1985 Absolute and convective instabilities in free shear layers. *J. Fluid Mech.* **159**, 151–168.

HUERRE, P. & MONKEWITZ, P. A. 1990 Local and global instabilities in spatially developing flows. *Ann. Rev. Fluid Mech.* **22**, 473–537.

HUNT, R. E. & CRIGHTON, D. G. 1991 Instability of flows in spatially developing media. *Proc. R. Soc. Lond.* A **435**, 109–128.

KARNIADAKIS, G. E. & TRIANTAFYLLOU, G. S. 1989 Frequency selection and asymptotic states in laminar wakes. *J. Fluid Mech.* **199**, 441–469.

KOCH, W. 1985 Local instability characteristics and frequency determination of self-excited wake flows. *J. Sound Vib.* **99**, 53–83.

LECORDIER, J. C., HAMMA, L. & PARANTHOEN, P. 1991 The control of vortex shedding behind heated cylinders at low Reynolds numbers. *Exps Fluids* **10**, 224–229.

LEDIZÈS, S., MONKEWITZ, P. A. & HUERRE, P. 1993 Weakly nonlinear analysis of spatially developing shear flows. In *Bluff-Body Wakes, Dynamics and Instabilities* (ed. H. Eckelmann, J. M. R. Graham, P. Huerre & P. A. Monkewitz), pp. 148–152. Springer.

LEDIZÈS, S., HUERRE, P., CHOMAZ, J.-M. & MONKEWITZ, P. A. 1994 Linear global modes in spatially-developing media. *Phil. Trans. R. Soc. Lond.* Submitted.

MATHIS, C., PROVANSAL, M. & BOYER, L. 1984 The Bénard–von Kármán instability: an experimental study near the threshold. *J. Phys. Lett. Paris* **45**, L483–L491.

MONKEWITZ, P. A. 1988 The absolute and convective nature of instability in two-dimensional wakes at low Reynolds numbers. *Phys. Fluids* **31**, 999–1006.

MONKEWITZ, P. A. 1989 Feedback control of global oscillations in fluid systems. *AIAA Paper* 89-0991.

MONKEWITZ, P. A. 1993 Wake control. In *Bluff-Body Wakes, Dynamics and Instabilities* (ed. H. Eckelmann, J. M. R. Graham, P. Huerre & P. A. Monkewitz), pp. 227–240. Springer.

MONKEWITZ, P. A., BERGER, E. & SCHUMM, M. 1991 The nonlinear stability of spatially inhomogeneous shear flows, including the effect of feedback. *Eur. J. Mech.* B/*Fluids* **10**(2) Suppl. 295–300.

MONKEWITZ, P. A., HUERRE, P. & CHOMAZ, J. M. 1993 Global linear stability analysis of weakly nonparallel shear flows. *J. Fluid Mech.* **251**, 1–20.

MONKEWITZ, P. A. & NGUYEN, L. N. 1987 Absolute instability in the near wake of two-dimensional bluff bodies. *J. Fluids Struct.* **1**, 165–184.

MORI, Y., HIJIKATA, K. & NOBUHARA, T. 1986 A fundamental study of symmetrical vortex generation behind a cylinder by wake heating or by splitter plate or mesh. *Intl J. Heat Mass Transfer* **29**, 1193–1201.

MORZYŃSKI, M. & THIELE, F. 1993 Numerical investigation of wake instabilities. In *Bluff-Body Wakes, Dynamics and Instabilities* (ed. H. Eckelmann, J. M. R. Graham, P. Huerre & P. A. Monkewitz), pp. 135–142. Springer.

NISHIOKA, M. & SATO, H. 1978 Mechanism of determination of the shedding frequency of vortices behind a cylinder at low Reynolds number. *J. Fluid Mech.* **89**, 49–60.

NOACK, B. R. 1992 Theoretische Untersuchung der Zylinderumstroemung mit einem niedrigdimensionalen Galerkin-Verfahren. *Rep.* 25/1992, Max-Planck-Institut fuer Stroemungsforschung, Goettingen.

NOACK, B. R. & ECKELMANN, H. 1994 A global stability analysis of the steady and periodic cylinder wake. *J. Fluid Mech.* **270**, 297–330.

NOTO, K., ISHIDA, H. & MATSUMOTO, R. 1985 A breakdown of the Kármán vortex street due to the natural convection. In *Flow Visualization III* (ed. W. J. Yang), pp. 348–352. Hemisphere.

OHLE, F. & ECKELMANN, H. 1992 Modeling of a Kármán vortex street at low Reynolds numbers. *Phys. Fluids* A **4**, 1707–1714.

PIERREHUMBERT, R. T. 1984 Local and global baroclinic instability of zonally varying flows. *J. Atmos. Sci.* **41**, 2141–2162.

PRANDTL, L. & TIETJENS, O. 1929 *Hydro- und Aeromechanik*. Springer.

PROVANSAL, M., MATHIS, C. & BOYER, L. 1987 Bénard–von Kármán instability: transient and forced regimes. *J. Fluid Mech.* **182**, 1–22.

RAGHU, S. & MONKEWITZ, P. A. 1991 The bifurcation of a hot round jet to limit-cycle oscillations. *Phys. Fluids* A **3**, 501–503.

RAMBERG, S. E. 1983 The effect of yaw and finite length upon the vortex wakes of stationary and vibrating circular cylinders. *J. Fluid Mech.* **128**, 81–107.

ROSHKO, A. 1954*a* On the development of turbulent wakes from vortex streets. *NACA Rep.* 1191.

ROSHKO, A. 1954*b* On the drag and shedding frequency of two-dimensional bluff bodies. *NACA TN* 3169.

ROUSSOPOULOS, K. 1993*a* Feedback control of vortex shedding at low Reynolds numbers. *J. Fluid Mech.* **248**, 267–296.

ROUSSOPOULOS, K. 1993*b* Aspects of bluff body wake control. In *Bluff-Body Wakes, Dynamics and Instabilities* (ed. H. Eckelmann, J. M. R. Graham, P. Huerre & P. A. Monkewitz), pp. 249–252. Springer.

SCHUMM, M. 1991 Experimentelle Untersuchungen zum Problem der absoluten und konvektiven Instabilitaet im Nachlauf zweidimensionaler stumpfer Koerper. PhD thesis D83-FB 09, Technical University Berlin. Published in *VDI – Fortschrittsberichte Reihe 7*, no. 196. Duesseldorf: VDI. Partial results have been published in 1988 by BERGER, E. & SCHUMM, M. Untersuchung der Instabilitaetsmechanismen in Nachlauf von Zylindern. *DFG Contractors Report* Be 343/18-1.

SOWARD, A. M. 1992 Thin disc kinematic $\alpha\omega$-dynamo models II. Short length scale modes. *Geophys. Astrophys. Fluid Dyn.* **64**, 201–225.

SREENIVASAN, K. R., RAGHU, S. & KYLE, D. 1989 Absolute instability in variable density round jets. *Exps Fluids* **7**, 309–317.

SREENIVASAN, K. R., STRYKOWSKI, P. J. & OLINGER, D. J. 1986 Hopf bifurcation, Landau equation and vortex shedding behind circular cylinders. In *Proc. Forum on Unsteady Flow Separation* (ed. K. N. Ghia), pp. 1–13. ASME.

STRYKOWSKI, P. J. & SREENIVASAN, K. R. 1990 On the formation and suppression of vortex shedding at low Reynolds number. *J. Fluid Mech.* **218**, 71–107.

STUART, J. T. 1971 Nonlinear stability theory. *Ann. Rev. Fluid Mech.* **3**, 347–370.

TOKUMARU, P. T. & DIMOTAKIS, P. E. 1991 Rotary oscillatory control of a cylinder wake. *J. Fluid Mech.* **224**, 77–90.

TRIANTAFYLLOU, G. S., TRIANTAFYLLOU, M. S. & CHRYSSOSTOMIDIS, C. 1986 On the formation of vortex streets behind stationary cylinders. *J. Fluid Mech.* **170**, 461–477.

TRITTON, D. J. 1959 Experiments on the flow past a circular cylinder at low Reynolds numbers. *J. Fluid Mech.* **6**, 547–567.

WEHRMANN, O. H. 1965 Reduction of velocity fluctuations in a Kármán vortex street by a vibrating cylinder. *Phys. Fluids* **8**, 760–761.

WILLIAMS, D. R., MANSY, H. & AMATO, C. W. 1992 The response and symmetry properties of a cylinder wake subjected to localized surface excitation. *J. Fluid Mech.* **234**, 71–96.

WILLIAMSON, C. H. K. 1989 Oblique and parallel modes of vortex shedding in the wake of a circular cylinder at low Reynolds numbers. *J. Fluid Mech.* **206**, 579–627.

WILLIAMSON, C. H. K. 1994 The transition to three-dimensionality in the wake of cylinders. *J. Fluid Mech.* (submitted).

WOOD, C. J. 1964 The effect of base bleed on a periodic wake. *J. R. Aeronaut. Soc.* **68**, 477–482.

WOOD, C. J. 1967 Visualization of an incompressible wake with base bleed. *J. Fluid Mech.* **29**, 259–272.

YU, M. H. & MONKEWITZ, P. A. 1990 The effect of nonuniform density on the absolute instability of two-dimensional inertial jets and wakes. *Phys. Fluids* A **3**, 1175–1181.